HHS Public Access

Author manuscript

*Nature*. Author manuscript; available in PMC 2023 May 15.

Published in final edited form as:

*Nature*. 2023 January ; 613(7945): 729–734. doi:10.1038/s41586-022-05587-z.

# Two broadly conserved families of polyprenyl-phosphate transporters

**Ian J. Roney**,

**David Z. Rudner***

Department of Microbiology, Harvard Medical School, 77 Avenue Louis Pasteur, Boston, MA 02115

## Summary paragraph:

Peptidoglycan and virtually all surface glycopolymers in bacteria are built in the cytoplasm on the lipid carrier undecaprenyl-phosphate (UndP)[1–4]. These UndP-linked precursors are transported across the membrane and polymerized or directly transferred to surface polymers, lipids, or proteins. UndP is then flipped to regenerate the pool of cytoplasmic-facing UndP. The identity of the flippase that catalyzes transport has eluded identification for decades. Here, using the antibiotic amphomycin that targets UndP[5–7], we discovered two broadly conserved protein families that affect UndP recycling. One (UptA) is a member of the DedA superfamily[8]; the other (PopT) contains the domain DUF368. Genetic, cytological, and syntenic analyses argue that these proteins are the missing UndP transporters. Importantly, homologs from gram-positive and gram-negative bacteria promote UndP transport in *Bacillus subtilis,* indicating that recycling activity is broadly conserved among family members. Inhibitors of these flippases could potentiate the current arsenal of cell envelope-targeting antibiotics.

Polyprenyl-phosphates are universal carriers of sugars and glycopolymers across membranes in all domains of life[1–4]. In bacteria, the 55-carbon isoprenoid undecaprenyl-phosphate (UndP or C55-P) is used to transport most glycopolymers across the cytoplasmic membrane including peptidoglycan (PG) precursors, O-antigens of lipopolysaccharide (LPS), teichoic acids, and capsule. UndP also ferries sugars and oligosaccharides across the membrane that are used to glycosylate lipid A of LPS, teichoic acids, and surface proteins (Extended Data Fig. 1). In eukaryotes and archaea the polyprenyl-phosphate, dolichol-phosphate (DolP) transports oligosaccharides across the membranes of the endoplasmic reticulum and the archaeal cytoplasmic membrane, respectively[1,2]. These DolP-linked sugars are then used to decorate membrane-anchored and secreted proteins. In all cases, the lipid carrier must be recycled via transport across the membrane. The flippases that catalyze polyprenyl-phosphate transport are among the last unknown enzymes in these pathways.

*Correspondence to: rudner@hms.harvard.edu.

Contributions

I.J.R and D.Z.R conceived of the study and I.J.R performed all experiments and analysis. D.Z.R supervised the study. I.J.R and D.Z.R wrote the paper.

Competing interests

The authors declare that they have no competing interests.

Bacterial cell wall biogenesis, the target of some of the most effective antibiotics, exemplifies these glycopolymer synthesis pathways (Fig. 1)[9]. A series of cytoplasmic enzymatic steps generate the PG precursor lipid II, a disaccharide pentapeptide linked to undecaprenyl-pyrophosphate (UndPP). Lipid II is then flipped to the outer leaflet of the cytoplasmic membrane where the muropeptide is polymerized and crosslinked into the cell wall meshwork. The UndPP product is dephosphorylated and UndP is flipped to the inner leaflet to complete the lipid II cycle (Fig. 1). During exponential growth, a bacterium contains ~$10^5$ UndP molecules that are thought to ferry a similar number of PG precursors across the cytoplasmic membrane every minute, suggesting that each lipid carrier is reused multiple times per cell cycle for PG synthesis alone[10,11]. *De novo* synthesis of UndP maintains the pool size during growth while recycling is the primary source for surface polymer biogenesis. Here, we define two broadly conserved families of flippases that catalyze UndP transport in bacteria and could function to recycle DolP in eukaryotes and archaea.

To screen for potential UndP flippases, we took advantage of the antibiotic amphomycin and its derivative MX2401[5–7] that bind the phosphate on UndP. Since these cyclic lipopeptides are unlikely to cross the membrane, they are thought to bind outward-facing UndP preventing its recycling and thus inhibit PG synthesis. We reasoned that over-expression of an UndP transporter would provide resistance to these antibiotics. We generated a *Bacillus subtilis* transposon library with a strong outward facing promoter[12] and plated the library on LB agar supplemented with MX2401 at concentrations above the minimum inhibitory concentration (MIC). The colonies were pooled and the transposon insertion sites mapped by transposon-sequencing (Tn-seq). Tn insertions were significantly over-represented at a single region of the genome and in all cases the outward-facing promoter faced the uncharacterized gene *yngC* (Fig. 2a). Over-expression of *yngC in B. subtilis* increased the MIC of MX2401 by >16-fold (Fig. 2b), validating our findings. Furthermore, deletion of *yngC* reduced the MIC 4-fold (Fig. 2b). These data suggest that YngC functions in UndP transport.

YngC is a member of the DedA superfamily, a broadly conserved but poorly understood family of membrane proteins found in all domains of life[8]. The AlphaFold-predicted structure of YngC resembles membrane transporters with membrane re-entrant loops on either side of the lipid bilayer[13] (Extended Data Fig. 2a). A conserved pair of arginines in one of these loops is required for MX2401 resistance (Extended Data Fig. 2b, Supplementary Figure 2a) and could function in phosphate binding. Interestingly, one of *yngC*'s promoters is regulated by the extracytoplasmic function (ECF) sigma factor $\sigma^{M}$ [14] (Extended Data Fig. 2e, f, g). This transcription factor is induced under conditions that trap UndP-linked intermediates and reduce the cellular pools of the lipid carrier[15]. Consistent with a role for $\sigma^{M}$ in regenerating this pool, a *sigM* mutant or a deletion of the $\sigma^{M}$-binding site in the *yngC* promoter sensitized *B. subtilis* to MX2401 (Extended Data Fig. 2h). Importantly, reducing *de novo* synthesis of UndP sensitized *B. subtilis* to loss of *yngC* (Extended Data Fig. 3a, b), providing further support for the idea that YngC recycles the lipid carrier.

*B. subtilis* encodes five additional DedA paralogs. Individual deletions in these genes did not affect the MIC of MX2401 (Extended Data Fig. 3c). A deletion of one of the paralogs, *ykoX*, modestly reduced the MIC of the Δ*yngC* mutant and a strain lacking all six paralogs phenocopied the Δ*yngC ΔykoX* double mutant (Fig. 2b). Thus, YngC is likely to be the principal *B. subtilis* DedA family member involved in UndP recycling. We note that over-expression of YkoX in the Δ*yngC* mutant provided some resistance to MX2401 (Fig. 2f and Extended Data Fig. 3d). These data raise the possibility that YkoX transports a distinct anionic lipid but can act on UndP when over-expressed.

Tn-seq screens in *Staphylococcus aureus* to profile the phenotypic responsiveness to 32 antibiotics identified transposon insertions upstream of two genes (*SAOUHSC_02816* and *00846*) when the Tn library was challenged with sub-inhibitory doses of amphomycin[16] (Extended Data Fig. 4a). *02816* encodes a DedA family member and *00846* encodes a protein with a domain of unknown function DUF368. We validated these uncharacterized hits and found that over-expression of either protein in *S. aureus* increased the MIC of MX2401 (Fig. 2c). Deletion of *02816* did not impact the MIC of MX2401 while deletion of *00846* reduced it by 4-fold (Fig. 2c). Strikingly, the MIC of the double mutant was ~256-fold lower than wild-type (Fig. 2c). Furthermore, the double mutant was growth-impaired, displayed cell size variability, and 10% of the cells had membrane permeability defects, consistent with impaired envelope assembly (Fig. 2de and Extended Data Fig. 4b, c). Over-expression of either *S. aureus* gene in *B. subtilis* lacking *yngC* and *ykoX* provided resistance to MX2401 (Fig. 2f). Since *B. subtilis* lacks a DUF368 homolog, these data suggest that the *S. aureus* DUF368 protein functions as an UndP transporter rather than a regulator or co-factor. DUF368 is a polytopic membrane protein that is widely conserved in bacteria and archaea (Supplementary Fig. 3). The AlphaFold-predicted structure of *S. aureus* DUF368 resembles canonical membrane transporters with 2-fold inverted symmetry and membrane re-entrant loops on either side of the lipid bilayer[13,17](Extended Data Fig. 2d, Supplementary Fig. 2b). The predicted gap between transmembrane helices 4 and 11 could allow the polyprenyl tail to remain in the lipid bilayer during transport of the phosphate head group, akin to the membrane-spanning groove in the eukaryotic TMEM16 and GPCR families[18,19] that transport lipids via the credit-card mechanism[20]. Based on the findings presented thus far and those below, we have renamed the DedA superfamily members encoded by *yngC* and *02816* UptA (UndP transporter A) and DUF368 proteins PopT (polyprenyl-phosphate transporter).

*S. aureus* encodes a second DedA paralog (*SAOUHSC_00901*) that was not identified in the Tn-seq screen described above. Over-expression of this gene in the *B. subtilis* Δ*uptA* Δ*ykoX* double mutant increased resistance to MX2401 by 4-fold (Fig. 2f), suggesting 00901 is also capable of UndP transport. Importantly, the *S. aureus* triple mutant lacking *uptA, popT* and *00901* was not viable (Fig. 2d), consistent with the requirement for UndP recycling in cell wall biogenesis. Furthermore, overexpression of UppS, responsible for *de novo* synthesis of UndP but not MurA that catalyzes the first committed step in PG precursor synthesis, largely suppressed the growth defect of the *S. aureus* Δ*uptA* Δ*popT* double mutant and restored viability to the triple mutant (Fig. 2g and Extended Data Fig. 4d), providing additional support for the idea that these factors recycle UndP. Finally, we determined the MICs of 12 antibiotics that target different steps in cell wall synthesis or other essential

processes in *B. subtilis* and *S. aureus* wild-type and their respective mutants. Virtually all of the MICs in a *B. subtilis* Δ*uptA* mutant were indistinguishable from wild-type, and most MICs were 1–2-fold lower in the *S. aureus* Δ*uptA* Δ*popT* double mutant compared to wild-type (Supplementary Table 1). The only exception was tunicamycin, which competes with inward-facing UndP for binding to MraY[21]. The *S. aureus* double mutant was highly susceptible to this drug, consistent with reduced levels of inward-facing UndP due to an accumulation of outward-facing UndP in the mutant. Collectively, these assays argue that the functions of UptA and PopT are specific to UndP recycling.

Gene neighborhood analysis[22] provides additional support for a role of these two protein families in UndP transport. In a subset of bacterial genomes, genes encoding a DedA superfamily member and a lipid phosphatase of the PAP2 family[23] are adjacent to each other; in others the two genes are fused (Fig. 3a and Extended Data Fig. 5a, b, c). Some PAP2 homologs, like *B. subtilis* BcrC and *E. coli* PgpB, are undecaprenyl-pyrophosphate phosphatases that convert surface-exposed UndPP to UndP prior to their transport to the cytoplasmic face of the membrane[24]. Similarly, in other bacterial genomes a gene encoding a DedA family member is present adjacent to *uppP* that encodes a second family of UndPP phosphatases[25] (Extended Data Fig. 5d, e). Accordingly, if these DedA paralogs transport UndP then the adjacent or fused genes would encode enzymes that catalyze sequential steps in the lipid II cycle (Fig. 1a). Analysis of all the *dedA* genes from two species in which one of the paralogs resides adjacent to a *pap2* or *uppP* gene is consistent with this model (Extended Data Fig. 5f, g). In the case of PopT, most archaeal genomes contain a cluster of genes required for surface protein glycosylation[26]. A DUF368-containing gene is also present in many archaeal genomes and 37% of the time is found in these clusters, often adjacent to an oligosaccharyltransferase of the *aglB* family (Fig. 3b and Extended Data Fig. 6a, b, c). The transfer of the lipid-linked oligosaccharide onto a surface protein by AglB liberates DolP that could then be recycled by the PopT homolog. Finally, gram-positive bacteria encode enzymes involved in glycosylating surface polymers and a DedA superfamily member is sometimes encoded in an operon with these enzymes. *B. subtilis* provides a prototypical example (Extended Data Fig. 6d). In this bacterium, a transcription factor controls the expression of two operons that are thought to be involved in glycosylation of lipoteichoic acids[27]. Four of the genes in these operons encode the full set of enzymes required to glycosylate this surface polymer. The fifth encodes UptA, which would complete the cycle in this sugar modification pathway (Extended Data Fig. 6e). Thus, gene neighborhood analysis suggests UptA and PopT family members are broadly conserved polyprenyl-phosphate transporters.

To directly test whether UptA and PopT family members function in UndP recycling, we conjugated a fluorescent dye to MX2401 (MX2401-FL) and used it to visualize UndP. Control experiments established that membrane labeling with MX2401-FL correlates with UndP levels (Extended Data Fig. 7a) and that the fluorescent probe cannot traverse the membrane and therefore reports on outward-facing UndP (Extended Data Fig. 7b). Wild-type *B. subtilis* cells expressing cytoplasmic blue fluorescent protein (BFP) and the Δ*uptA* Δ*ykoX* double mutant expressing mCherry were mixed, labeled with MX2401-FL, and visualized by fluorescence microscopy. Wild-type cells had faint MX2401-FL signal along the cytoplasmic membrane while cells lacking the two DedA paralogs had ~2-fold higher

membrane fluorescence (Fig. 4a and Extended Data Fig. 7c, Extended Data Fig. 8a, b). Importantly, the MX2401-FL signal in the *B. subtilis* double mutant was dramatically reduced when UptA$^{Bs}$, UptA$^{Sa}$, or PopT$^{Sa}$ was over-expressed (Fig. 4a and Extended Data Fig. 7c). In an analogous experiment, we labeled wild-type *S. aureus* and the Δ*uptA* Δ*popT* double mutant with spectrally distinct Fluorescent D-amino acids (FDAAs)[28] and then mixed the two cultures and stained with MX2401-FL. The double mutant had strong MX2401-FL fluorescence while the signal was barely detectable in wild-type (Fig. 4a and Extended Data Fig. 7c). Similar results were obtained when MX2401 was labeled with three other fluorescent dyes including Alex Fluor 488, which prevents membrane permeation of its conjugates[29–31] (Extended Data Fig. 9a, b, c).

*E. coli* encodes eight DedA superfamily members[8]. The mutants have pleiotropic phenotypes that include defects in cell division, morphology, alkaline tolerance, membrane potential, and antibiotic resistance[8,32–34]. The proteins have been hypothesized to function as proton-dependent transporters that help maintain the proton motive force[8,35]. We note that the PMF was intact in *B. subtilis* Δ*uptA Δykox* and the *S. aureus uptA* Δ*popT* double mutants (Extended Data Fig. 10). To investigate whether any of the *E. coli* DedA paralogs catalyze UndP transport, we expressed each in *B. subtilis* and tested for MX2401 resistance. Although several increased the MIC of MX2401 of the *B. subtilis* Δ*uptA* Δ*ykoX* mutant by ~2–4-fold, only one conferred high-level resistance (Fig. 4b and Extended Data Fig. 9d). This DedA paralog (DedA) is the founding member of the superfamily and is most similar to UptA$^{Bs}$ and UptA$^{Sa}$ (Supplementary Figure 2a and Supplementary Table S2a). We extended this cross-species complementation analysis to a diverse collection of UptA and PopT homologs. The DedA superfamily members tested were chosen based on their similarity to the validated UptA family members. In addition to UptA$^{Sa}$ and UptA$^{Ec}$, homologs from *Acinetobacter baumannii*, *Pseudomonas aeruginosa*, and *Bacillus cereus* conferred MX2401 resistance to the *B. subtilis* double mutant (Fig. 4b). Similarly, expression of PopT homologs from *Bacillus cereus*, *Streptococcus pneumoniae*, *Vibrio cholerae*, *Borrelia burgdorferi*, and *Corynebacterium glutamicum* increased the MIC of MX2401 (Fig. 4c). Importantly, all five of the proteins tested also reduced surface-exposed UndP as assayed by MX2401-FL (Extended Data Fig. 8c, d).

We conclude that UptA and PopT family members catalyze the transport of UndP, the final step in virtually all cell envelope biogenesis and surface modification pathways in both gram-positive and gram-negative bacteria. Their discovery completes the parts list for many of these intensively studied pathways and represents a new set of targets to potentiate the current arsenal of antibiotics.

The mechanisms of UndP transport by UptA and PopT are currently unknown. Recent *in vitro* reconstitution experiments of two eukaryotic DedA superfamily members TMEM41B and VMP1[36] were found to redistribute fluorescently labeled phospholipids with diverse headgroups from the luminal to the exposed face of proteoliposomes. Lipid transport was energy independent suggesting that these transporters function as lipid scramblases. Our work has uncovered a role for UptA and PopT in retrograde transport of UndP but we cannot exclude a model in which UptA or PopT act as scramblases. If correct, the transfer of sugars onto the lipid carrier on the cytoplasmic face of the membrane would result

in concentration-driven retrograde transport. Future work will focus on characterizing the mechanism of UndP transport of UptA and PopT *in vitro*. Interestingly, depletion of either TMEM41B or VMP1 in tissue culture cells led to defects in the sorting of cholesterol, phosphatidylserine, and phosphatidylcholine suggesting these proteins function in lipid transport *in vivo*[36,37]. The analysis of UptA family members presented here strengthens this conclusion and suggests that other bacterial DedA superfamily members function in lipid transport. Based on our analysis of the *B. subtilis* DedA paralogs, we hypothesize that *in vivo* these transporters have more narrow substrate specificity and act on distinct lipids. Furthermore, it is tempting to speculate that a DedA superfamily member recycles DolP in eukaryotes while PopT homologs transport DolP in archaea.

Other than an increase in surface-exposed UndP, the *B. subtilis* Δ*uptA* Δ*ykoX* double mutant had no discernable growth or morphological defects while the *S. aureus* Δ*uptA* Δ*popT* double mutant was growth-impaired and the triple mutant was inviable. These data raise the possibility that *B. subtilis* encodes a third family of UndP transporters or that UndP flipping can occur spontaneously albeit inefficiently. We favor the latter model because a screen using a transposon with an even stronger outward-facing promoter did not identify additional hits when the *B. subtilis* Δ*uptA* Δ*ykoX* double mutant was challenged with MX2401. Furthermore, no genes were identified as synthetic lethal with the single or double *B. subtilis* mutants. UppP has been hypothesized to function as both an UndPP phosphatase and an UndP transporter[3,38] but over-expression or deletion of *uppP* or *bcrC* in *B. subtilis* had no impact on the MIC of MX2401 (Extended Data Fig. 9e) and neither gene was identified as a hit in our Tn-seq screen nor the one performed in *S. aureus* (Extended Data Fig. 4a). These observations lead us to hypothesize that UndP can spontaneously flip/flop in the cytoplasmic membrane and that the extent of protonation of the phosphate headgroup influences efficiency. Transmembrane pH gradients have been shown to cause asymmetric distribution of phosphatidic acid within artificial bilayers[39] and the pH gradient maintained by the PMF could similarly lead to an asymmetry of UndP. This model could also explain why the Δ*popT* Δ*uptA* synthetic lethality observed in *Vibrio cholerae* was suppressed in acidic conditions[40]. However, at this stage we cannot rule the possibility that additional families of transporters contribute to UndP recycling and will continue screening for these factors in the future.

Although not essential, the DedA superfamily member that is most similar to *E. coli* DedA ($UptA^{Ec}$) in *Neisseria meningitidis, Klebsiella pneumoniae* and *Burkholderia thailandensis* (Supplementary Table 2b) is required for intrinsic resistance to the last-resort antibiotic colistin[35,41,42]. Loss-of-function mutations in the associated genes in these gram-negative pathogens confer colistin-sensitivity and in some cases it has been shown that expression of $UptA^{Ec}$ can reverse this sensitivity, implicating UndP transport. Colistin resistance is mediated by aminoarabinose (Ara4N) modification to lipid A of LPS, which reduces its affinity for polycationic antibiotics[43]. The Ara4N modification is built on UndP in the cytoplasm, flipped to the periplasm and then transferred to lipid A. Mutations in these DedA superfamily members result in low levels of Ara4N-modified lipid A[35] and we hypothesize that the reduction in UndP recycling in these mutants accounts for the decreased modification. UptA homologs in *Klebsiella pneumoniae* and *A. baumannii* are also required for resistance to complement-mediated killing and *K. pneumoniae* UptA is

additionally required for neutrophil evasion in a mouse model for lung colonization[44–46]. Long O-antigen chains and a thick capsule, both glycopolymers that are built on UndP, are primary defense mechanisms of these pathogens. Thus, small molecules that target UptA and PopT transporters could potentiate both last resort antibiotics and host defense mediated killing.

## Methods

### General methods

All *Bacillus subtilis* strains were derived from the prototrophic strain PY79[1]. All *B. subtilis* experiments were performed at 37 °C with aeration in lysogeny broth (LB). Antibiotic concentrations used were: 100 μg/mL spectinomycin, 10 μg/mL kanamycin, 5 μg/mL chloramphenicol, 10 μg/mL tetracycline, 1 μg/mL erythromycin and 25 μg/mL lincomycin (MLS). Isopropyl ß-d-thiogalactopyranoside (IPTG) was used at a concentration of 500 μM unless indicated otherwise. All experiments with MX2401 or amphomycin used media supplemented with 25 μg/mL $CaCl_2$. All *B. subtilis* strains were generated using the one-step competence method unless indicated otherwise. All *Staphylococcus aureus* strains were derived from RN4220. Cells were grown at 37 °C with aeration in Tryptic soy broth (TSB). Antibiotic concentrations used were: 7.5 μg/mL erythromycin, 50 μg/mL kanamycin, 450 μg/mL spectinomycin, 5 μg/mL chloramphenicol. Anhydrotetracycline (aTc) was used at a concentration of 100 ng/mL unless indicated otherwise. Transductions were performed using phage 80alpha. All strains, plasmids, oligonucleotides, and synthetic DNA used in this study can be found in Supplementary Tables S3–S6.

### Statistics and reproducibility

All MIC experiments were performed in at least biological triplicate and representative images are shown. All microscopy analyses were performed in at least biological duplicate with many fields of view analyzed and representative images are shown. Spot assays and streak analysis were performed in at least biological triplicate. Western blotting was performed in biological duplicate. Attempts at replication for all experiments was successful.

### Transposon mutagenesis and suppressor isolation

Transposon libraries were generated as described previously[2], libraries were generated using pIR242, an *E. coli - B. subtilis* shuttle vector containing a temperature-sensitive replicon for *B. subtilis*, the mariner-Himar1 transposase, and a spectinomycin resistance cassette followed by a strong outward-facing promoter (P*pen*) and flanked by inverted repeats recognized by the transposase. The pIR242 plasmid was separately transformed into BIR769 or BIR672 and plated on LB agar supplemented with MLS and incubated at 30 °C. Transformants were inoculated into LB supplemented with spectinomycin and grown with aeration at 22 °C for 24 hours. Cultures were pooled and frozen with 15% glycerol. Aliquots of the frozen stocks were thawed and plated onto LB agar supplemented with spectinomycin, $CaCl_2$ and 2.5 μg/mL MX2401 (BIR769) or 0.3 μg/mL MX2401 (BIR672). Plates were incubated at 42 °C overnight to select for transposon mutagenized cells that had lost the plasmid and provided resistance to MX2401.

### Mapping transposon insertion sites

Sequencing and mapping of the transposon insertion sites was performed as described previously[2,3]. Briefly, transposon-mutagenized colonies that grew on LB agar supplemented with MX2401 were pooled, and genomic DNA extracted. DNA was digested with MmeI and ligated to adaptors. Transposon-chromosome junctions were amplified by PCR and the products were size selected using a 2% agarose gel. The Illumina MiSeq platform was used to sequence the library. Sequencing reads were mapped to the *B. subtilis* 168 chromosome (NCBI NC_00964.3) using Bowtie 1.0.0. All NGS datasets generated in this work have been deposited to the NCBI sequence read archive within project PRJNA898639 (SAMN31619234 and SAMN31619233). Re-analysis of TN-seq data from *Santiago et al.* 2018[4] was performed as described in their methods using sequences previously deposited on the NCBI sequence read archive (SRX3390726).

### Minimal inhibitory concentration (MIC) assays

Exponentially growing cultures of *B. subtilis* or *S. aureus* were back-diluted 1:1000 into 96-well microtiter plates containing the indicated concentrations of antibiotic and inducers. Plates were sealed with breathable membranes and grown with orbital shaking at 37 °C overnight. Plates were photographed after the overnight (~16 hr) incubation.

### Spot-dilution assays

Late-log cultures were normalized to OD600=1 and 10-fold serial dilutions were generated. 5 μL of each dilution were spotted onto LB agar supplemented with or without IPTG or onto TSB agar supplemented with or without aTc, IPTG or 3ug/mL fosfomycin. Plates were incubated at 37 °C overnight and photographed the next day.

### Genomic Neighborhood Analysis

The Enzyme Similarity Tool (EFI-EST v2.0) from the Enzyme Function Initiative[5] (available at: https://efi.igb.illinois.edu/efi-est/) was used to generate sequence similarity networks (SSN) for the DedA and DUF368 protein families from the pfam entries SNARE_assoc (PF09335) and DUF368 (PF04018) respectively. Due to the large size of the SNARE_assoc family, the UniRef90 database was used. The SSNs were then used as inputs for performing genomic neighborhood analysis using the Enzyme Function Initiative Genome Neighborhood Tool[5] (EFI-GNT v1.0) available at: https://efi.igb.illinois.edu//efi-gnt/index.php. Alignment score cutoffs of 35% were used for both analyses. Gene neighborhood diagrams (GND) were generated to visualize the 10 nearest genes surrounding all *dedA* and *duf368* members. An SSN was also generated for the subset of DUF368 members in archaea, this dataset was used as an input for performing gene neighborhood analysis and the resulting gene neighborhood networks (GNN) were uploaded and visualized in cytoscape. Cytoscape 3.8.2 was used to examine and quantify the genes most found within a 10 gene window of *duf368*.

### MX2401-FL

MX2401 has a single primary amine[6] and drug optimization efforts have found that it can be modified without loss of potency. MX2401 was labeled at this position with three

dyes reported to be membrane impermeable CF488A, CF405M, and CF594 using the Mix-n-Stain CF Dye Small Ligand Labeling Kit (Biotium #92350, 92362, 92352) following the manufacturer's instructions. Briefly, 10 µL (0.1 µmol) of MX2401 dissolved in DMSO was mixed with 2 µL of reaction buffer. The mixtures were added to individual dyes and briefly vortexed. The reactions were incubated for 30 minutes in the dark at room temperature. 2 µL of quenching buffer was added to the reactions, briefly vortexed and incubated for 5 minutes in the dark. DMSO was added to a final volume of 100 µL generating 1 mM solutions of MX2401-CF488A, -CF405M, and -CF594. MX2401 was labeled with Alex Fluor 488 (AF488) using Alexa Fluor 488 TFP ester kit (ThermoFisher cat# A37570) following the manufacturer's instructions with minor modifications. Briefly, 100 µg of Alexa Fluor 488 TFP ester was dissolved in 10 µL of DMSO and added to 1 mg of MX2401 dissolved in 100 µL of 0.1 M HEPES pH 8.2. The mixture was incubated with shaking for 1 hour in the dark at room temperature. To quench the reaction 10 µL of 1M Tris pH 7 was added to the reaction and was incubated with shaking for 1 additional hour in the dark at room temperature.

### MX2401-FL labeling and fluorescence microscopy

Exponentially growing cultures of *S. aureus* were incubated for 20 minutes with the fluorescent D-amino acids (FDAAs) HADA (Tocris) or RADA (Tocris) at final concentrations of 100 µM. Exponentially growing cultures of *Bacillus subtilis* and FDAA labelled *S. aureus* were collected by centrifugation at 7000 RPM for 2 min. Cells were washed once with 1xPBS (pH 7.4) and re-suspended in $1/25^{th}$ volume of 1xPBS. MX2401-FL was added to a final concentration of 25 µM and incubated for 30 seconds. Cells were washed with 1xPBS, resuspended in 1/25 volume of 1xPBS, and spotted onto 1.5% agarose pads containing growth medium. Propidium iodide, TMA-DPH and FM-464 labeling were performed in 1xPBS at final concentrations of 5 µM.

Phase and fluorescence microscopy was performed with a Nikon Ti inverted microscope using a Plan Apo 100x/1.4 Oil Ph3 DM objective, a Lumencore SpectraX LED illumination system and an Andor Zyla 4.2 Plus sCMOS camera. Chroma ET filter cubes (#49000, 49002, 49003 and 49008) were used for imaging BFP/HADA/TMADPH, MX2401-FL, YFP and mCherry/RADA/Propidium Iodide/FM464 respectively. Exposure time of 50 ms was used for HADA, RADA, Propidium Iodide and mCherry; 400 ms was used for BFP; 200 ms was used for MX2401-FL, FM464 and TMADPH and 1 s was used for YFP. Images were acquired with Nikon elements 4.3 software and analyzed using ImageJ (version2.3).

### Fluorescence microscopy quantification

ImageJ was used to quantify fluorescent intensities. For quantification of PyngC-yfp a vegetatively expressed blue fluorescent protein (BFP) was used to identify cell boundaries. Intensity values from the YFP channel were extracted and the background autofluorescence from an empty field of view was subtracted from the image. For quantification of MX2401-FL labeling, cells were co-stained with MX2401-FL and FM464. FM464 was used to identify cell membranes. Single pixel wide lines were drawn down the sidewalls of cells, avoiding overlapping cells and double membranes at septa. Average intensity values for each sidewall were extracted from the MX2401-FL channel. Background autofluorescence was

taken as an average from five places in each field of view and subtracted from each intensity measurement. GraphPad Prism 9 was used for plotting.

### Structural model visualization

Alphafold2 predictions of PopT (SAOUHSC_00846) and UptA (YNGC_BACSU) were downloaded from the AlphaFold Protein Structure Database (available at: https://alphafold.ebi.ac.uk/). ChimeraX1.3 was used to visualize the structural models and generate images. Reentrant helixes are highlighted in blue and red. Arginine residues critical for YngC ($UptA^{Bs}$) function are shown as sticks.

### Immunoblot analysis

Immunoblot analysis was performed as described previously[7]. Briefly, 1mL of exponentially growing cells were normalized by OD600 and harvested by centrifugation (2 min at 7000 RPM). The cell pellet was resuspended in lysis buffer (20 mM Tris pH 7.0, 10 mM $MgCl_2$, 1mM EDTA, 1 mg/mL lysozyme, 10 μg/mL DNase I, 100 μg/mL RNase A, 1 mM PMSF, 1 μg/mL leupeptin, 1 μg/mL pepstatin) and incubated at 37 °C for 15 minutes. An equal volume of sample buffer (0.25 M Tris pH 6.8, 4% SDS, 20% glycerol, 10 mM EDTA, 10% β-mercaptoethanol) was added to the lysis reactions and vortexed briefly to complete lysis. Proteins were separated by SDS- PAGE on 12.5% polyacrylamide gels, transferred onto Immobilon-P membranes (Millipore) by electrophoretic transfer and blocked with 5% Milk in phosphate buffered saline with 0.5% Tween-20 (PBS-T). The blocked membranes were probed with monoclonal anti-His (1:4,000) (Genscript) or polyclonal anti-SigA (1:10,000)[8] antibodies diluted into 3% BSA in PBS-T. Primary antibodies were detected using horseradish peroxidase-conjugated goat anti-rabbit IgG (1:3,000) (BioRad) or goat anti-mouse IgG (1:20,000) (BioRad) and the Super Signal chemiluminescence reagent as described by the manufacturer (Pierce).

### Dendrograms

Dendrograms were made using AnnoTree version 1[9]. All entries of pf04018 (DUF368) were mapped to representative dendrograms of bacteria and archaea. Hits are shown as blue lines.

### Multiple Sequence Alignment

Multiple sequence alignments were performed using Clustal Omega version 1.2.4 [10] and visualized with Espript 3.0[11].

## Extended Data

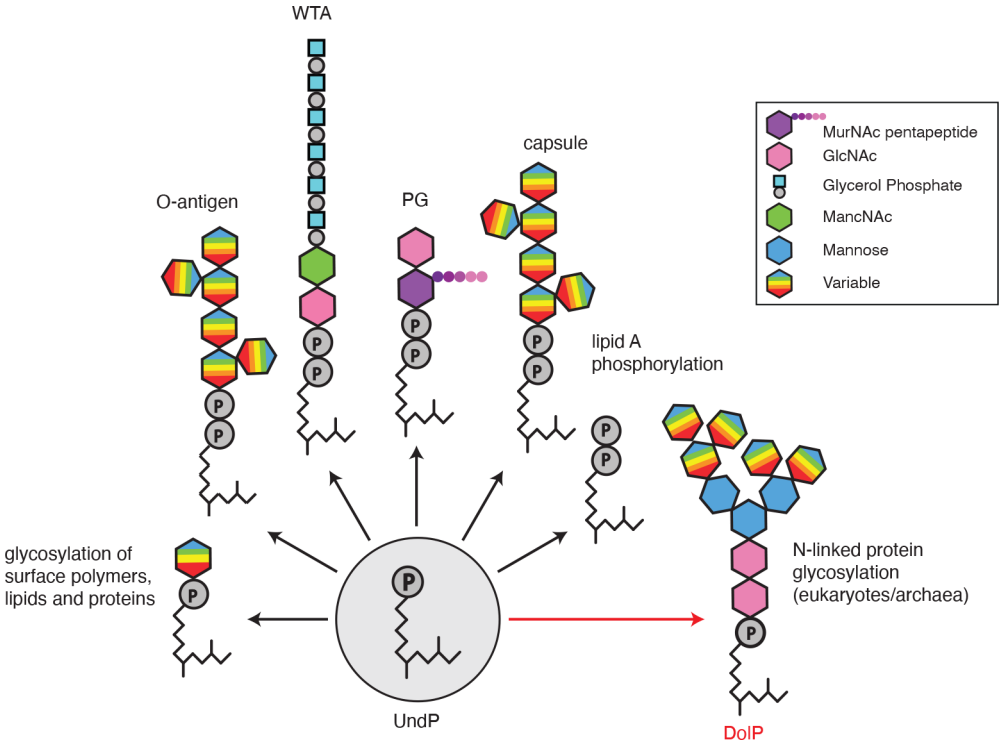


**Extended Data Fig. 1. Polyprenyl-phosphate lipids are universal transporters of surface glycopolymers.**

Schematic illustrating the glycopolymers and sugar modifications that are assembled on undecaprenyl-phosphate (UndP) in bacteria and on dolichol-phosphate (DolP) in archaea and eukaryotes. Although an oligosaccharide carried on DolP is shown, some eukaryotes use the pyrophosphate carrier (DolPP).

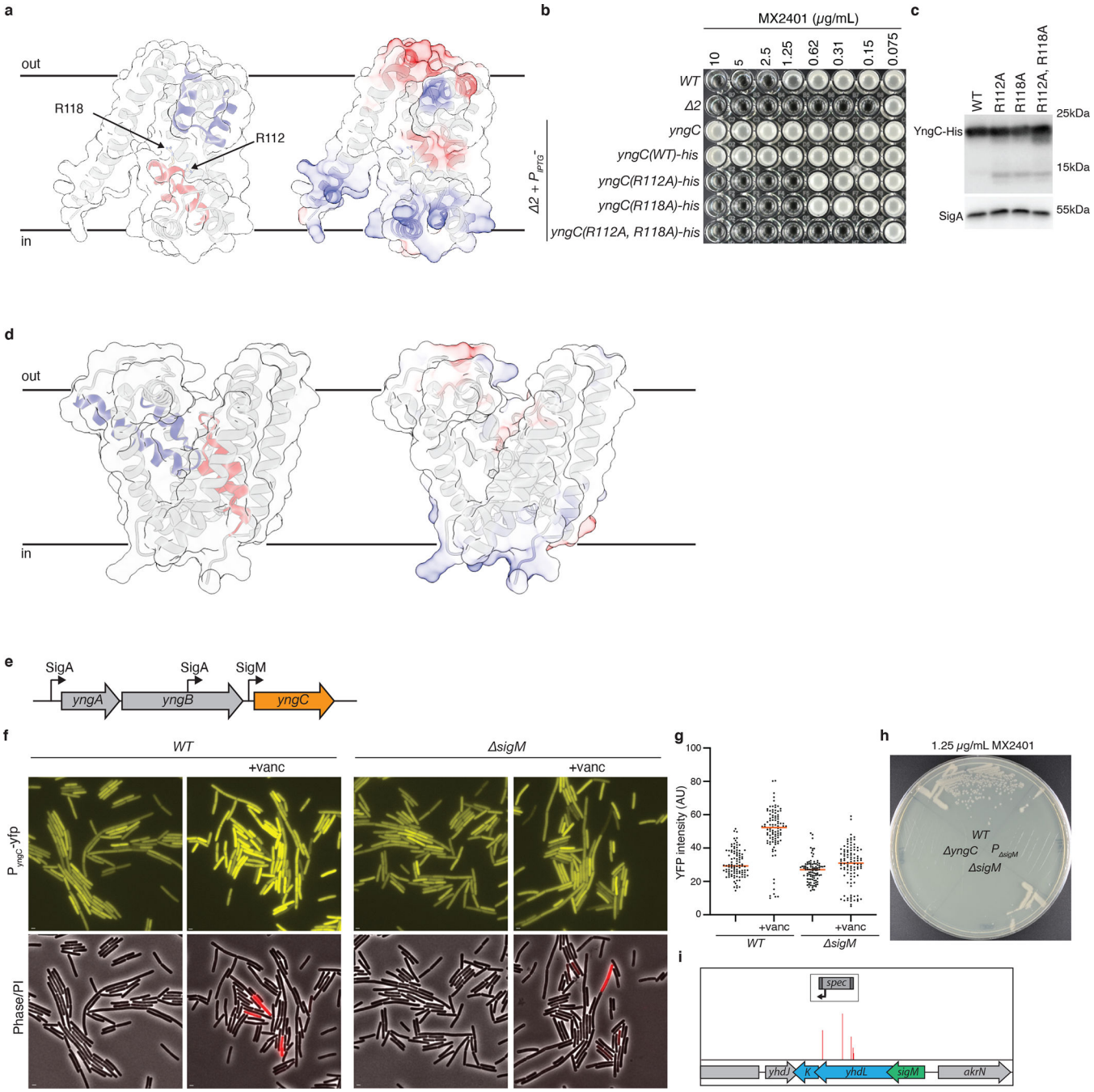


**Extended Data Fig. 2. YngC has features of membrane transporters and is expressed under $\sigma^M$ control.**

Structural models of YngC **(a)** and SAOUHSC_00846 **(d)** as predicted by AlphaFold2. (Left) Membrane re-entrant helices are highlighted in red and blue. Conserved arginines in the red re-entrant helix of YngC are indicated. (Right) Surface charge distribution in the predicted structures. **(b)** Minimum inhibitory concentration (MIC) assays of the indicated *B. subtilis* strains with point mutations in the conserved arginines in *yngC*. **(c)** Immunoblot analysis of YngC-His levels using anti-His antibodies of the strains in (b). SigA is the sample processing control. **(e)** Schematic of the *yngABC* operon highlighting the promoters

that regulate *yngC* expression. Two are recognized by sigma factor A ($\sigma^A$) and one is recognized by the ECF sigma factor M ($\sigma^M$). **(f)** Representative fluorescence images of cells harboring a transcriptional fusion of the *yngC* $\sigma^M$ promoter to *yfp*. YFP fluorescence increases in cells exposed to vancomycin for 30 minutes, a condition that activates $\sigma^M$. The reporter is not induced by vancomycin in a Δ*sigM* mutant. Scale bar, 1 μm. **(g)** Quantification of YFP fluorescence from 100 cells of the strains and conditions in (f). Bar represents the median. **(h)** Streaks of the indicated strains on LB agar supplemented with 1.25 μg/mL MX2401. $P_{\Delta sigM}$ contains a deletion of the $\sigma^M$ promoter of *yngC*. **(i)** The Tn-seq screen for MX2401 resistance mutants identified insertions in the genes (*yhdL* and *yhdK*) encoding the anti-$\sigma^M$ factors, consistent with increased $\sigma^M$-dependent transcription of *yngC* providing MX2401 resistance. Transposon insertion profile at the indicated *B. subtilis* genomic region is shown. Each vertical line indicates an insertion site; its height reflects the number of reads at this position (maximum height ≥5,000). The transposon insertion site with the maximum number of reads in this region had 2,600 reads. For comparison, the insertion sites adjacent to *yngC* had >20,000 reads.

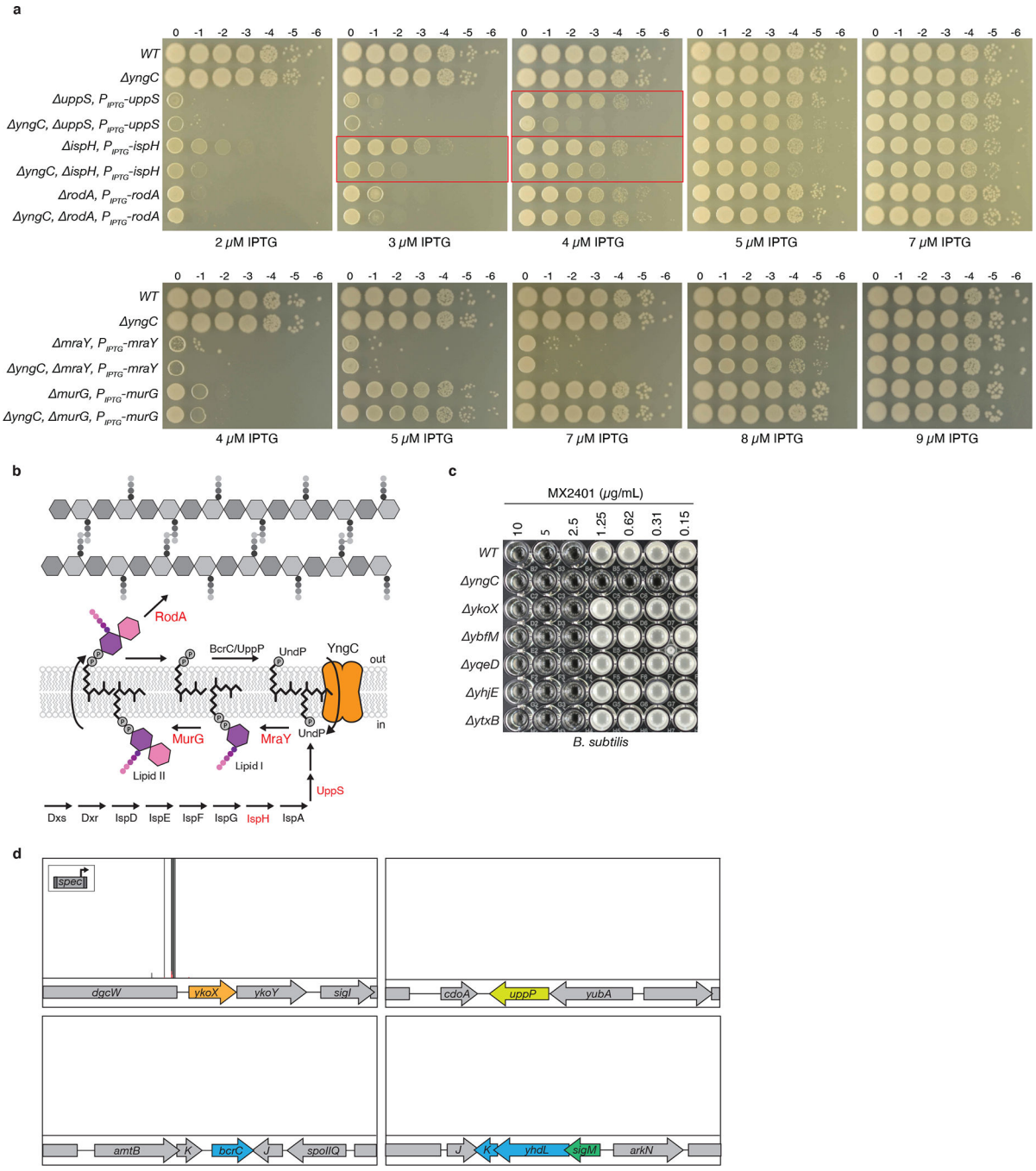


**Extended Data Fig. 3. Δ*yngC* sensitizes *B. subtilis* to reduced levels of UndP synthesis.**
**(a)** Spot-dilutions of the indicated *B. subtilis* strains with IPTG-regulated alleles on LB agar supplemented with the indicated concentrations of IPTG. Strains with reduced levels of IspH or UppS are sensitive to the absence of *yngC.* Relevant comparisons are boxed in red. Strains with reduced levels of RodA, MurG or MraY grow similarly in the presence or absence of *yngC*. **(b)** Schematic of the UndP synthesis pathway illustrating the two sources of UndP for lipid II biogenesis: *de novo* synthesis and recycling. Enzymes shown in red were expressed at reduced levels in the assays in (a). **(c)** Minimum inhibitory

concentration (MIC) of MX2401 in the indicated *B. subtilis* strains, each lacks one of the six DedA paralogs. **(d)** The *B. subtilis* Δ*yngC* mutant was mutagenized with a transposon carrying a strong outward facing $P_{pen}$ promoter (insert). The library was plated on LB agar supplemented with 0.3 μg/mL MX2401 to select for mutants that provide resistance. Transposon insertion profiles at the indicated *B. subtilis* genomic regions are shown. Each vertical line indicates an insertion site; its height reflects the number of sequencing reads at this position (maximum height ≥5000). The average number of reads was >40,000. The majority of insertions mapped upstream of the *ykoX* gene in an orientation that would increase its transcription. Transposon insertions were not enriched upstream of *bcrC* or *uppP* that encode UndPP phosphatases, suggesting that these proteins do not have UndP transport activity, as was proposed previously[3,38]. Unlike the Tn-seq screen in a wild-type (*yngC*+) background, in the Δ*yngC* mutant, transposon insertions were not enriched in the genes (*yhdL* and *yhdK*) encoding the anti-$\sigma^M$ factors, consistent with the model that their inactivation provides increased MX2401 resistance by increasing $\sigma^M$-dependent transcription of *yngC*.

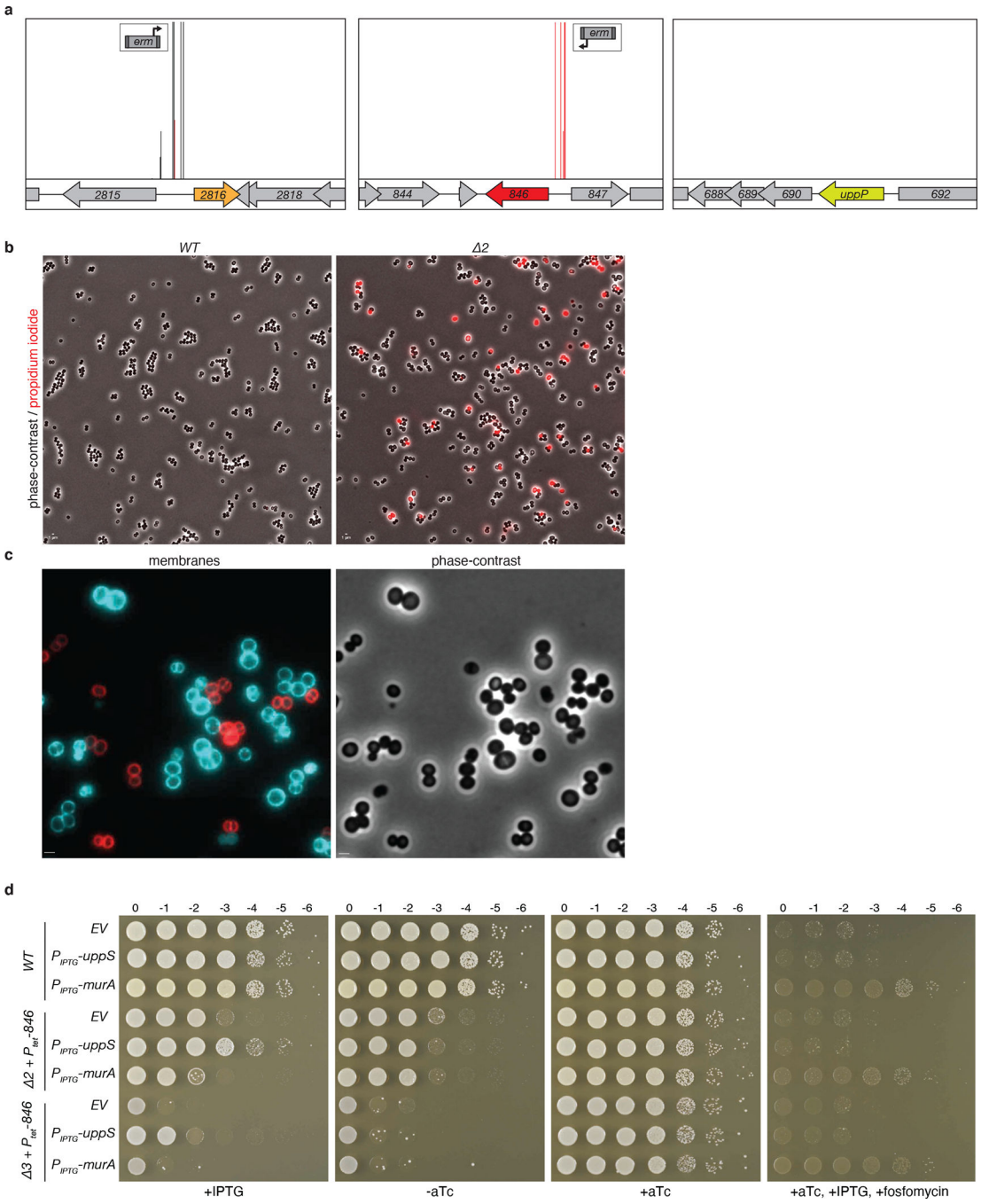


**Extended Data Fig. 4. A transposon-sequencing screen identified insertions upstream of *02816* and *00846* that confer resistance to amphomycin in *S. aureus*.**

**(a)** Reanalysis of Tn-seq data from *Santiago et al.* 2018[16]. A library of *S. aureus* mutagenized with a transposon carrying a strong outward facing promoter ($P_{tuf}$) was grown in sub-inhibitory concentrations of amphomycin (9.6 μg/mL). Transposon insertion profiles at the indicated *S. aureus* genomic regions are shown. Each vertical line indicates an insertion site; its height reflects the number of reads at this position (maximum height ≥2,000). Most transposon insertions mapped upstream of *SAOUHSC_02816* and

*SAOUHSC_00846* in orientations that are predicted to increase transcription of these genes. By contrast, insertions were not enriched upstream of the UndPP phosphatase *uppP*, suggesting that this membrane phosphatase does not have UndP transport activity, as previously proposed [3,38]. **(b)** Representative micrographs of wild-type and the Δ2 (Δ*uptA* Δ*popT*) double mutant. Shown are overlays of phase-contrast and fluorescence images of propidium iodide-stained cells. Quantification of the PI-positive cells from several fields of view (>1,000 cells per strain) yielded a PI-positive rate of 0.1% for wild-type and 10% for the Δ*uptA* Δ*popT* mutant. **(c)** Wild-type and Δ2 cells were stained with fluorescent membrane dyes FM-464 (red) and TMA-DPH (blue), respectively, and then mixed and imaged on the same agarose pad. Scale bar, 1 μm. **(d)** Spot-dilutions of the indicated *S. aureus* strains harboring an empty vector (EV) or a vector with an IPTG-regulated promoter fused to *uppS* or *murA*. The Δ2 *(Δ00846 Δ02816*) and Δ3 *(Δ00846 Δ02816 Δ00901*) strains have an aTc-regulated allele of *00846* (846). In the presence of 500 μM IPTG the Δ2 strain overexpressing UppS grows similarly to wild-type and the Δ3 strain is able to form tiny colonies at all dilutions. By contrast, the growth of the two mutants overexpressing MurA phenocopies the mutants with the empty vector. Overexpression of MurA enables growth on LB agar plates supplemented with 3 μg/mL fosfomycin.

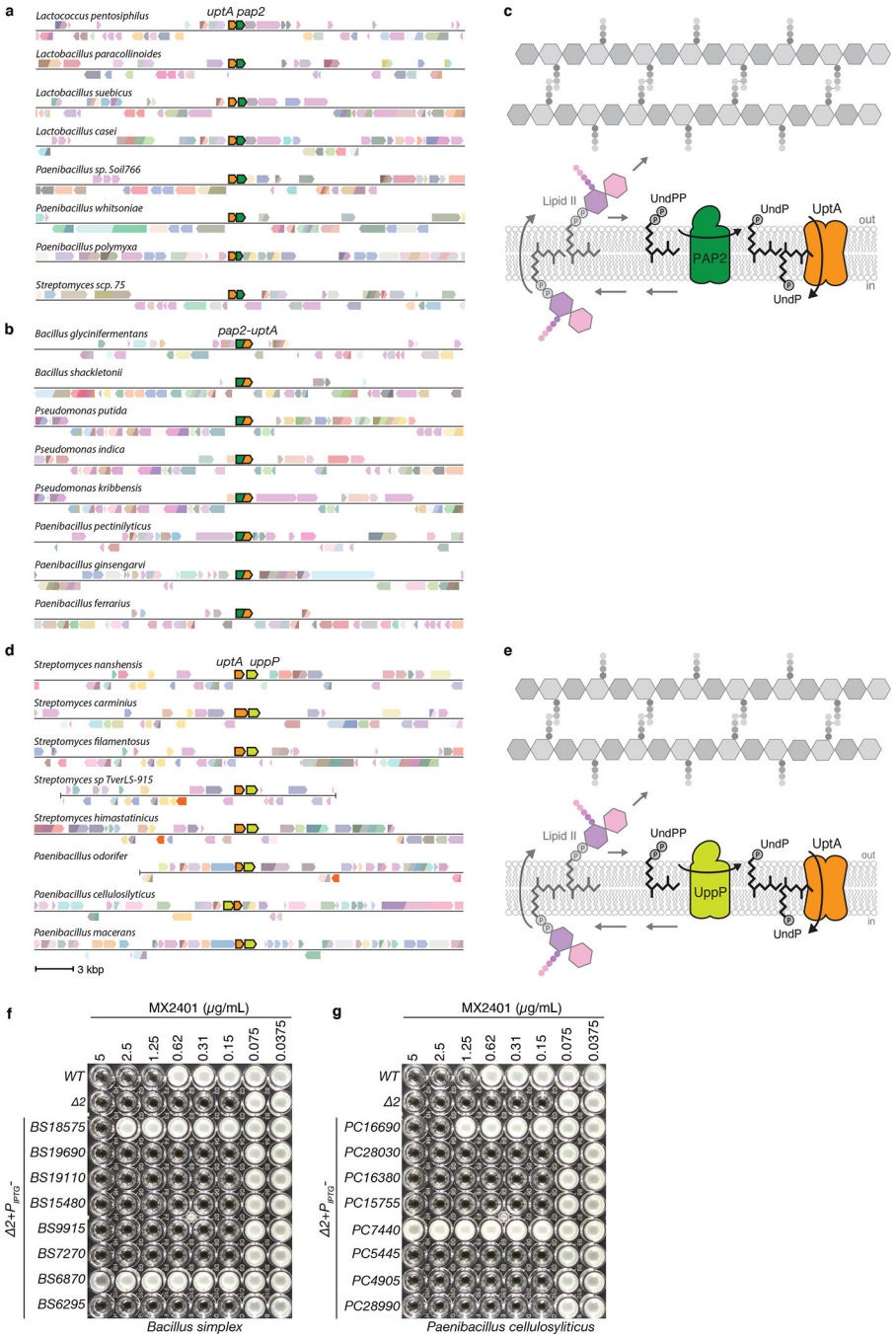


**Extended Data Fig. 5. Gene neighborhood analyses reveal that *dedA* paralogs can be found adjacent to or fused with *pap2* lipid phosphatases or adjacent to *uppP* undecaprenyl-pyrophosphate phosphatases.**

Representative genomic neighborhood analyses showing synteny **(a)** and gene-fusions **(b)** of DedA family members with PAP2 lipid phosphatases. **(c)** Schematic of the lipid II cycle highlighting the role of PAP2 family members like BcrC and DedA family members like YngC (UptA) in dephosphorylating UndPP and flipping UndP across the membrane, respectively. **(d)** Representative genomic neighborhood analysis showing synteny of *dedA* transporters with the undecaprenyl-pyrophosphate phosphatase *uppP*. Most examples of

synteny between *dedA* and *uppP* genes are from *Streptomycetes* and *Paenibacilli* genomes. **(e)** Schematic of the lipid II cycle highlighting the role of UppP family members and DedA family members like YngC (UptA) in dephosphorylating UndPP and flipping UndP across the membrane, respectively. MIC assays of the indicated *B. subtilis* strains lacking *uptA* and *ykoX* (Δ2) expressing one of the eight *Bacillus simplex* **(f)** or *Paenibacillus cellulosyliticus* **(g)** DedA paralogs. *BS18575* is adjacent to a *pap2* gene in *B. simplex*. *PC16690* is adjacent to a *uppP* gene in *P. cellulosyliticus*. Strains were grown in LB with 500 μM IPTG in the presence of the indicated concentration of MX2401. Uniprot IDs for the proteins included in the genome neighborhood diagrams can be found in Supplementary Table 3.

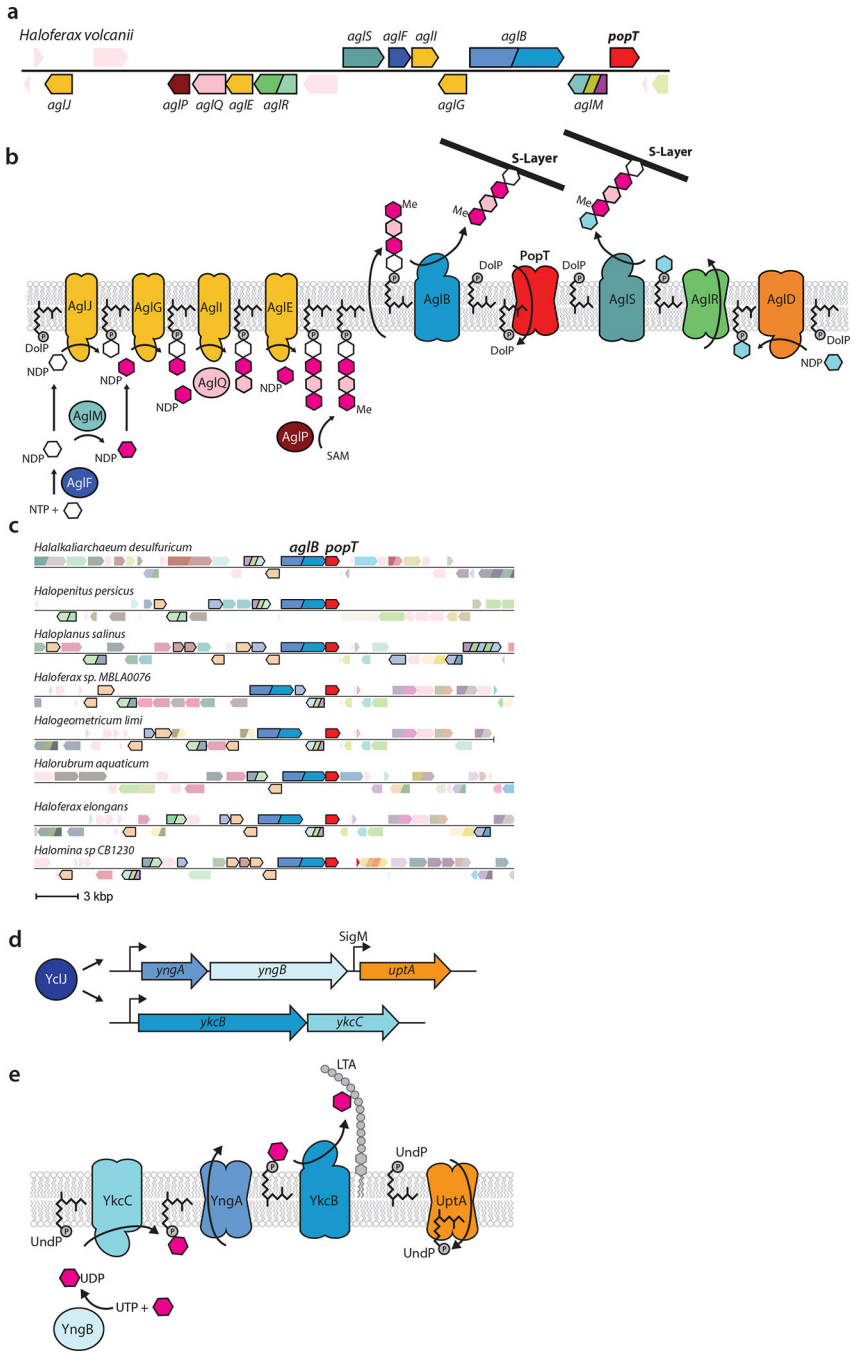


**Extended Data Fig. 6. Gene neighborhood analysis indicates that *duf368* genes are often present in archaeal gene clusters involved in S-layer protein glycosylation.**

**(a)** Representative genomic neighborhood from *Haloferax volcanii* with all the characterized genes involved in S-layer protein glycosylation and *popT* highlighted. **(b)** Schematic of the S-layer protein glycosylation pathway encoded in the *H. volcanii* gene cluster based on *Jarrel et al. 2014*[26]. PopT is hypothesized to catalyze the recycling of DolP to complete the cycle. AglR is shown flipping one of the two UndP-linked sugars but could transport both. **(c)** Gene neighborhood analysis showing synteny of *duf368* (*popT*) transporters with *aglB*

and other genes involved in N-linked protein glycosylation (outlined in black). Uniprot IDs for the proteins included in this diagram can be found in Supplementary Table 3. **(d)** Cartoon depiction of the regulation of the *yngABC* and *ykcBC* operons by the transcription factor YclJ[54]. **(e)** Schematic of the putative cell surface glycosylation pathway encoded by YclJ regulon members[27]. YngA is a member of the GtrA flippase family that transports UndP-linked monosaccharides across the cytoplasmic membrane. YngB is a member of the UDP glucose pyrophosphorylase family and has been shown to charge sugars with UDP groups[27]. YkcB is a member of the glycosyltransferase-39 family that transfers monosaccharides from the UndP carrier to surface polymers and is thought to glycosylate lipoteichoic acid (LTA). YkcC is a member of the glycosyltransferase-2 family that adds UDP charged monosaccharides onto UndP on the cytoplasmic leaflet of the membrane. The DedA paralog YngC (UptA) is proposed to complete the cycle.

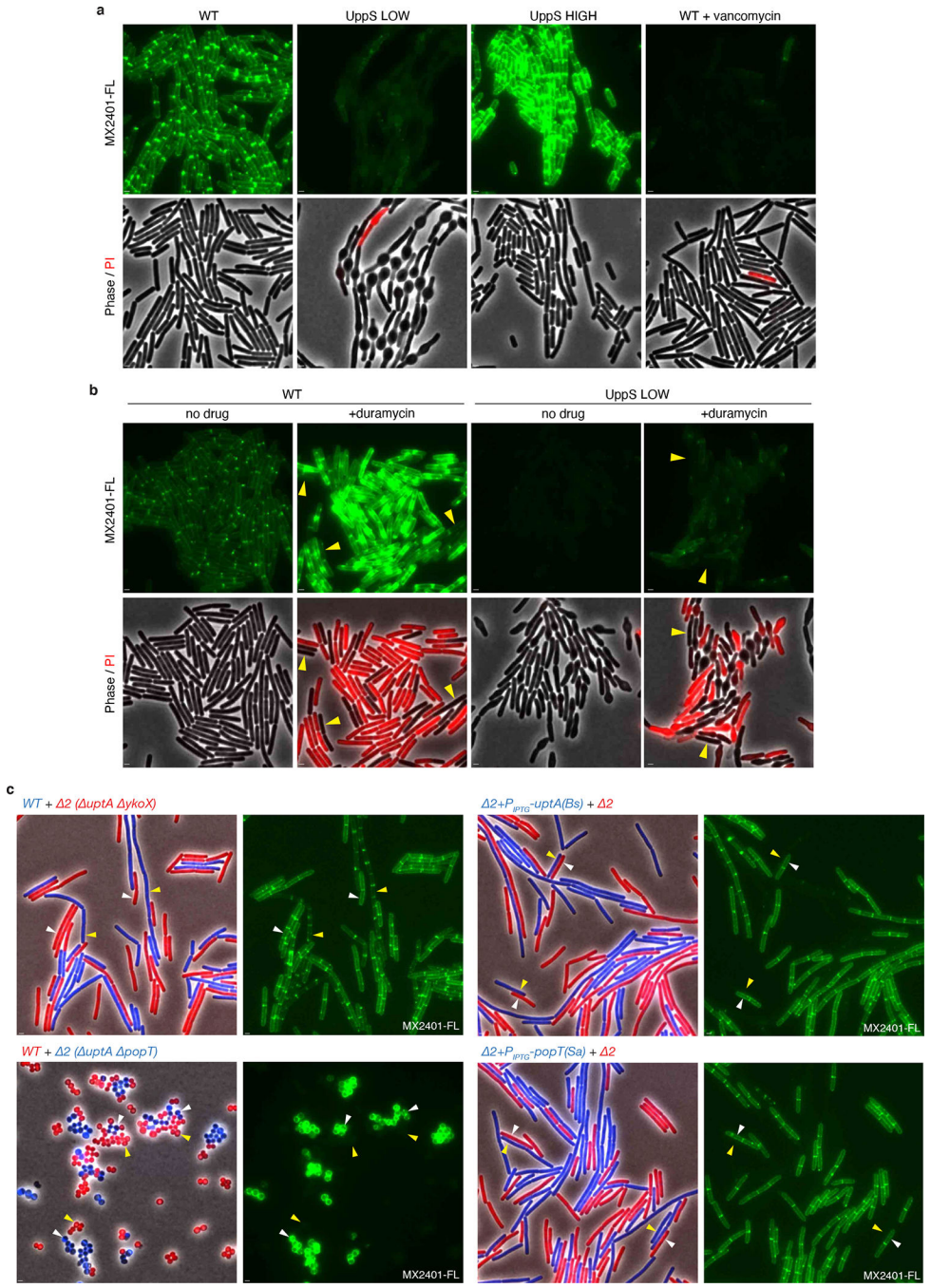


**Extended Data Fig. 7. MX2401-FL specifically labels outward-facing UndP.**

**(a)** Validation of MX2401 conjugated to CF488 (MX2401-FL). Representative fluorescence and phase-contrast images of the indicated strains labeled with MX2401-FL and propidium iodide (PI). Cells with reduced *de novo* synthesis of UndP (UppS LOW) harbor an IPTG-regulated allele of *uppS* (Pspank-*uppS*) and were propagated in the presence of 4 μM IPTG. Cells with increased *de novo* synthesis of UndP (UppS HIGH) harbor a stronger IPTG-regulated allele of *uppS* (Physpank-*uppS*) and were propagated with 500 μM IPTG. UppS LOW cells have low MX2401-FL staining and bulge due to impaired for cell wall

synthesis. UppS HIGH cells have high MX2401-FL staining and are shorter. Cells treated with vancomycin for 5 minutes prior to MX2401-FL staining trap UndP in lipid II and have low MX2401-FL signal. All MX2401-FL images were normalized identically with minimum and maximum intensities of 125 and 600 to detect weak MX2401-FL staining in the UppS LOW and vancomycin-treated strains. **(b)** Wild-type and UppS LOW strains were stained with MX2401-FL or a mixture of MX2401-FL and duramycin, which generates pores in the membrane allowing MX2401-FL access to the cytoplasmic-facing UndP. Cells with membrane permeability defects as assayed by PI have higher MX2401-FL signal. Cells with intact membranes (yellow carets) have lower MX2401-FL staining. All MX2401-FL images were normalized identically with minimum and maximum intensities of 125 and 1500 to prevent saturating the MX2401-FL signal. **(c)** Representative microscopy images of the indicated strains. Strains expressing different fluorescent proteins (*B. subtilis*) or labeled with different fluorescent D-amino acids (*S. aureus*) were mixed and then stained with MX2401-FL. (Left) overlays of phase contrast and fluorescent images in the red and blue channels to distinguish the two strains. (Right) MX2401-FL staining. Yellow carets highlight wild-type cells or cells over-expressing UptA(*Bs*) or PopT(*Sa*). White carets highlight cells lacking the UndP transporters. Scale bar, 1 μm.

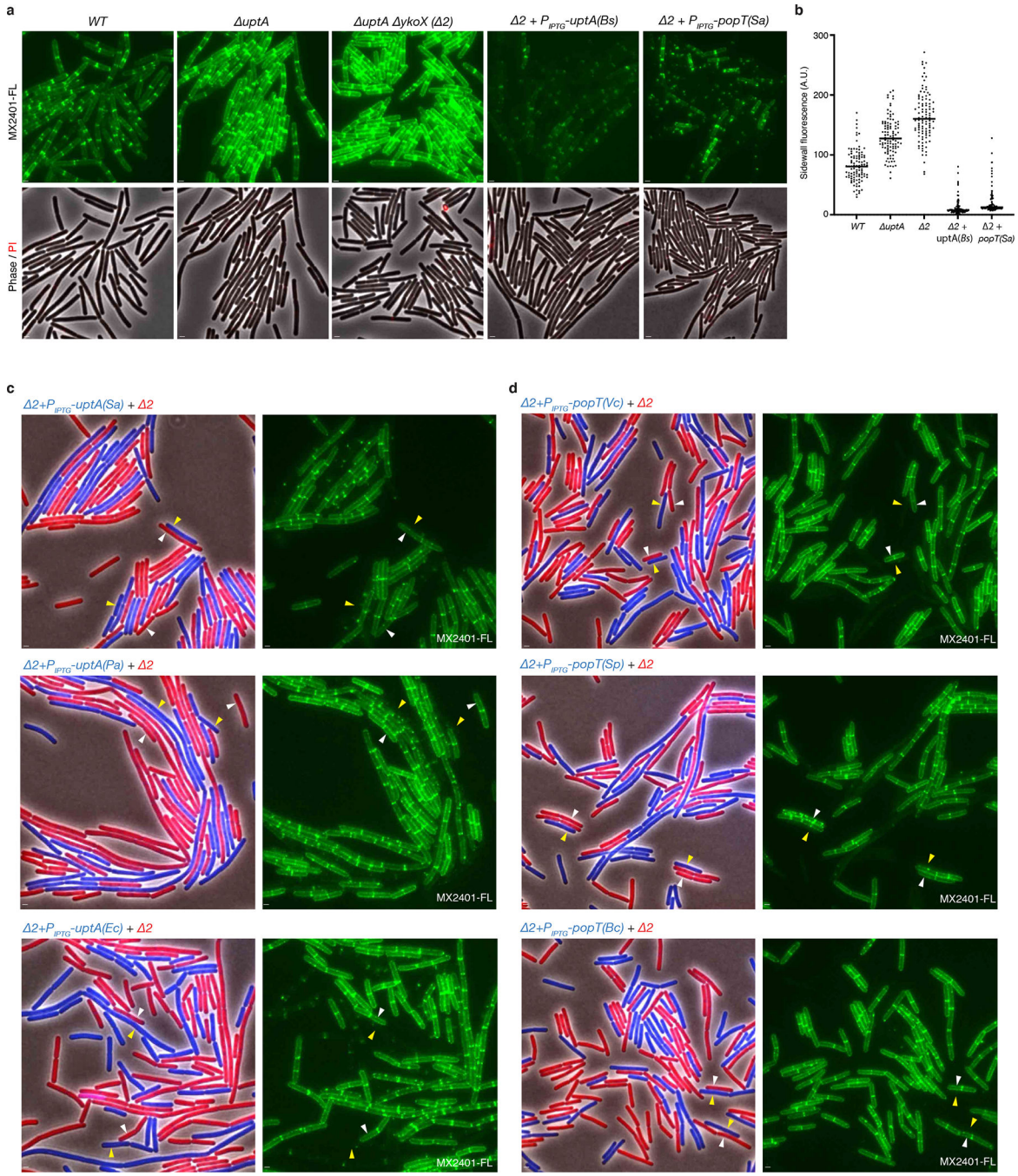


**Extended Data Fig. 8. UptA and PopT expression reduces MX2401-FL surface labeling.**

**(a)** Representative fluorescence and phase-contrast images of the indicated *B. subtilis* strains labeled with MX2401-FL and propidium iodide. The strains with IPTG-regulated *popT* and *uptA* alleles were grown in the presence of 500 μM IPTG. **(b)** Quantification of MX2401-FL labeling from the strains imaged in (a). Fluorescence intensity measurements of the sidewalls of 100 cells of each genotype were determined and plotted. Bar represents the median. **(c)** Representative images of the indicated *B. subtilis* strains. Two strains expressing different fluorescent proteins were mixed and then stained with MX2401-FL.

The left panels show overlays of phase contrast and fluorescent images in the red and blue channels to distinguish the two strains. The right panels show MX2401-FL staining. Yellow carets highlight cells over-expressing an UptA homolog from *S. aureus* (*Sa*), *Pseudomonas aeruginosa* (*Pa*), and *E. coli* (*Ec*) in a strain lacking *uptA* and *ykoX* (Δ2). White carets highlight cells lacking *uptA* and *ykoX*. **(d)** Yellow carets highlight cells over-expressing a PopT homolog from *Vibrio cholerae* (*Vc*), *Streptococcus pneumoniae* (*Sp*), or *Bacillus cereus* (*Bc*) in a strain lacking *uptA* and *ykoX* (Δ2). White carets highlight cells lacking *uptA* and *ykoX*. Scale bar, 1 μm.

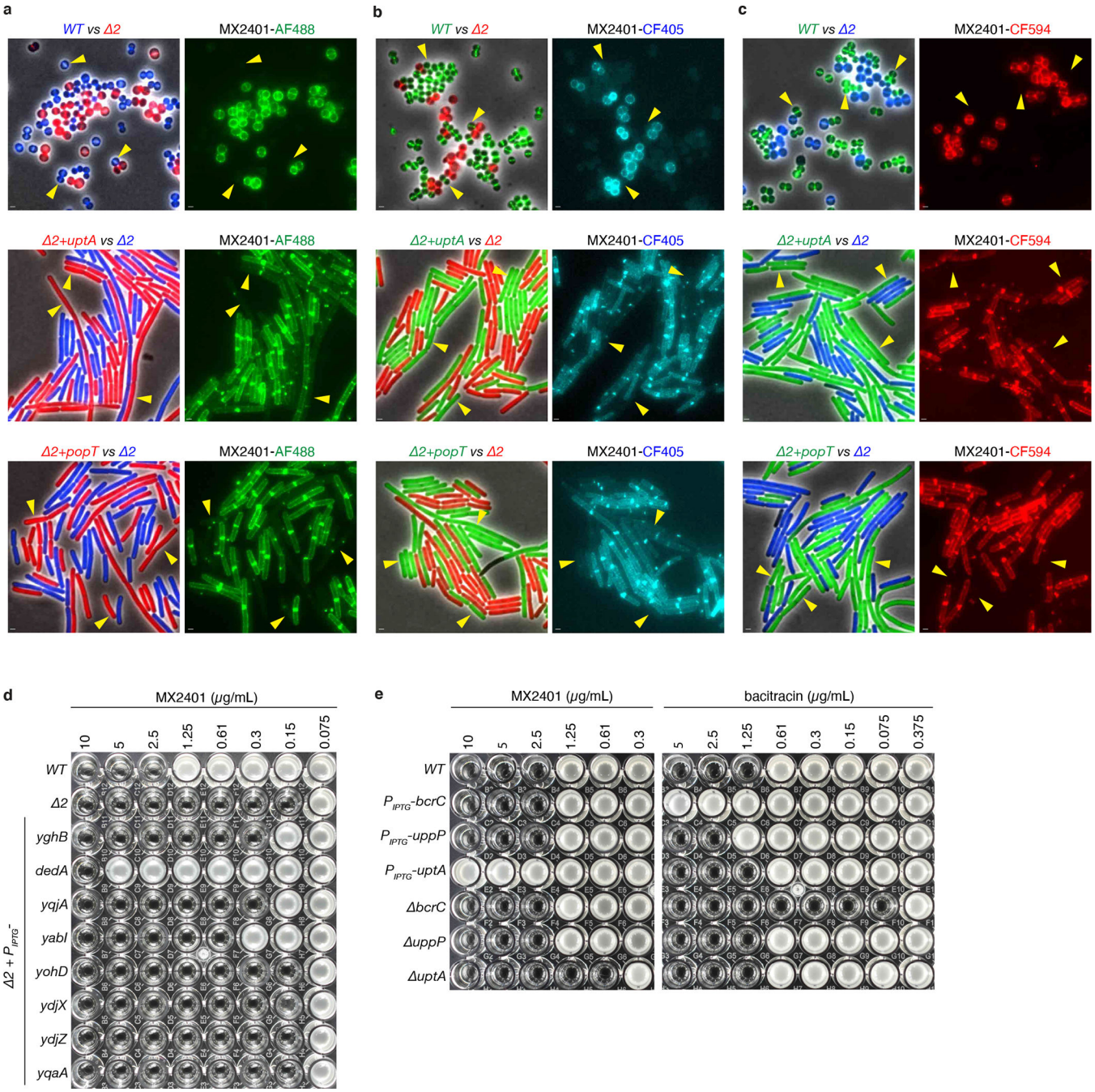


**Extended Data Fig. 9. MX2401 conjugated to three different fluorescent dyes stains cells similarly.**

Representative images of the indicated *B. subtilis* or *S. aureus* strains. Two strains expressing different fluorescent proteins (*B. subtilis*) or labeled with different fluorescent D-amino acids (*S. aureus*) were mixed and then stained with MX2401 labeled with **(a)** Alexa Fluor 488 (MX2401-AF488), **(b)** CF405 (MX2401-CF405), and **(c)** CF594 (MX2401-CF594). Alexa Fluor 488 prevents membrane permeation of its conjugates[30,31]. CF405 and CF594 are also reported to be membrane-impermeable by the manufacturer (Biotium). The left panels show overlays of phase-contrast and fluorescence images in the

red and blue, red and green, or green and blue channels to distinguish the two strains. The right panels show MX2401-FL staining. Yellow carets highlight wild-type cells or cells over-expressing UptA*(Bs)* or PopT*(Sa)*. All three fluorescently labeled MX2401 probes yield similar results. Scale bar, 1 μm. **(d)** MIC assays of the indicated strains each expressing one of the eight *E. coli* DedA paralogs in *B. subtilis* lacking *uptA* and *ykoX* (Δ2). Strains were grown in LB with 10 μM IPTG. At 500 μM, cells expressing YqjA and YabI had 4-fold higher MICs (≥8-fold lower than cells expressing DedA). **(e)** Over-expression or deletion of the undecaprenyl-pyrophosphate phosphatase genes *uppP* or *bcrC* in *B. subtilis* do not alter the MIC of MX2401. MIC assays of the indicated *B. subtilis* strains tested with MX2401 and separately with bacitracin that targets UndPP. These experiments were performed in a strain background deleted for the bacitracin efflux pump (Δ*bceAB*).

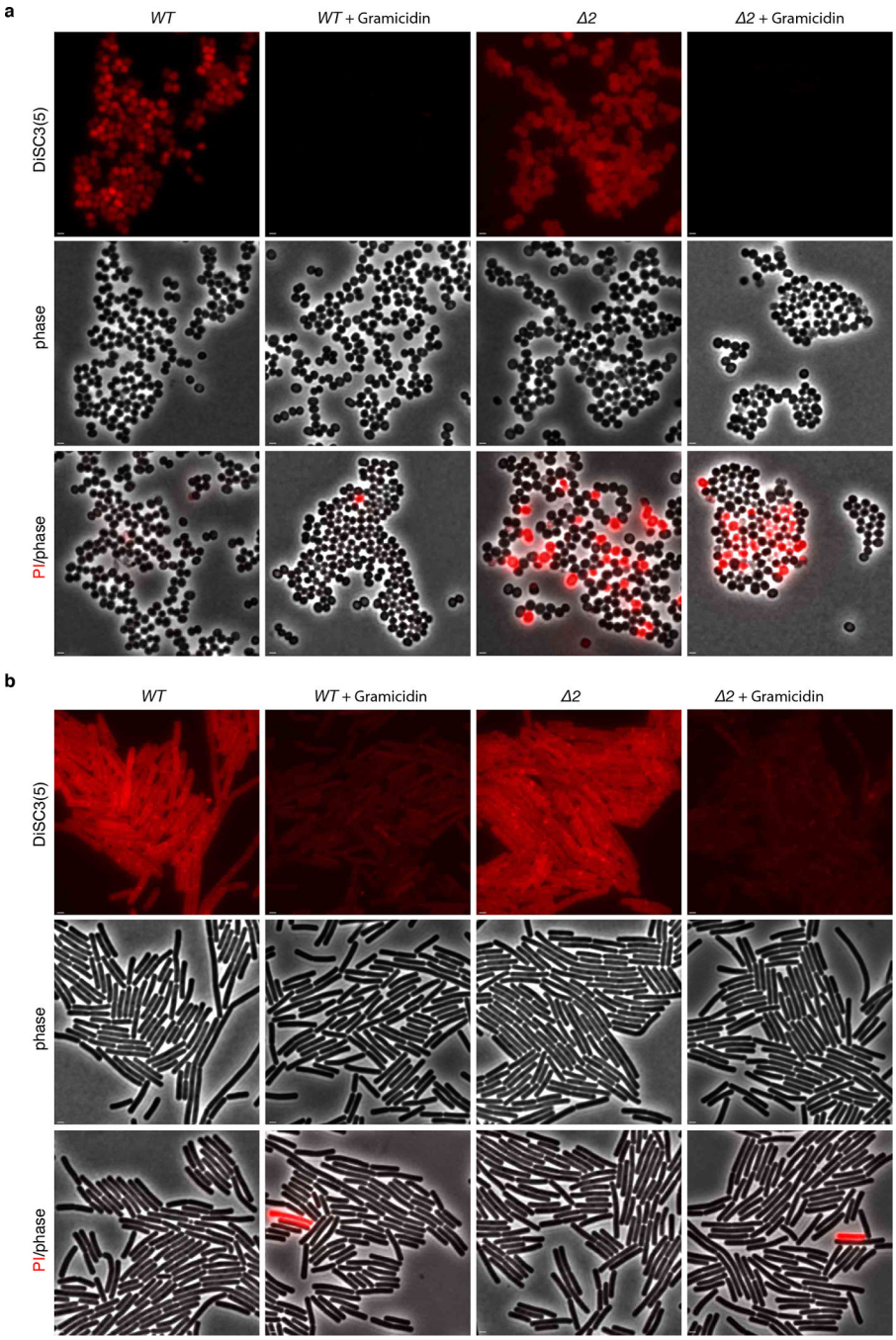


**Extended Data Fig. 10. *S. aureus* and *B. subtilis* cells lacking UndP transporters remain polarized.**

**(a)** Representative fluorescence and phase-contrast images of *S. aureus* wild-type and the *ΔpopT ΔuptA* (Δ2) mutant. The two strains were stained with the potentiometric dye 3,3'-Dipropylthiadicarbocyanine Iodide (DiSC3(5)). Treatment with the ionophore Gramicidin that depolarizes membranes was used as a positive control. The same cultures were separately stained with propidium iodide (PI) to assess the percentage of cells with membrane permeability defects. **(b)** Representative images of wild-type and the *ΔuptA*

*ΔykoX* (Δ2) *B. subtilis* mutant stained with DiSC3(5). Gramicidin was used as a positive control for loss of membrane potential. Scale bar, 1 μm.

## Supplementary Material

Refer to Web version on PubMed Central for supplementary material.

## Acknowledgements:

We thank all members of the Bernhardt-Rudner super-group for helpful advice, discussions, and encouragement, Tom Bernhardt, Suzanne Walker, Andrew Kruse for insights and advice, Susan Farmer and Bob Hancock for MX2401, the MicRoN core for advice on microscopy, and Matt Waldor for coordinating submission. Support for this work comes from the National Institute of Health Grants GM086466, GM127399, GM145299, U19 AI109764 (D.Z.R.).

## Data availability

NGS datasets generated in this study have been uploaded to the NCBI Sequence read archive within project PRJNA898639 (SAMN31619234 and SAMN31619233). Reads were mapped to *B. subtilis* genome (NCBI NC_00964.3). NGS datasets that were reanalyzed from Santiago et al. 2018 can be found on the NCBI Sequence read archive (SRX3390726) and the analysis was conducted as described in the paper. Raw data for all graphs has been uploaded as source data. Uniprot accession codes for gene neighborhood analysis can be found in supplementary tables. Primers, synthetic DNA constructs and strains used can be found in supplementary tables.

## References

1. Rush JS, Gao N, Lehrman MA & Waechter CJ Recycling of Dolichyl Monophosphate to the Cytoplasmic Leaflet of the Endoplasmic Reticulum after the Cleavage of Dolichyl Pyrophosphate on the Lumenal Monolayer*. J Biol Chem 283, 4087–4093 (2008). [PubMed: 18077451]
2. Eichler J & Guan Z Lipid sugar carriers at the extremes: The phosphodolichols Archaea use in N-glycosylation. Biochimica Et Biophysica Acta Bba - Mol Cell Biology Lipids 1862, 589–599 (2017).
3. Workman SD & Strynadka NCJ A Slippery Scaffold: Synthesis and Recycling of the Bacterial Cell Wall Carrier Lipid. J Mol Biol 432, 4964–4982 (2020). [PubMed: 32234311]
4. Manat G et al. Deciphering the Metabolism of Undecaprenyl-Phosphate: The Bacterial Cell-Wall Unit Carrier at the Membrane Frontier. Microb Drug Resist 20, 199–214 (2014). [PubMed: 24799078]
5. Tanaka H, Ōiwa R, Matusukura S & Ōmura S Amphomycin inhibits phospho-N-acetylmuramyl-pentapeptide translocase in peptidoglycan synthesis of Bacillus. Biochem Bioph Res Co 86, 902–908 (1979).
6. Rubinchik E et al. Mechanism of Action and Limited Cross-Resistance of New Lipopeptide MX-2401. Antimicrob Agents Ch 55, 2743–2754 (2011).
7. Singh M, Chang J, Coffman L & Kim SJ Solid-state NMR characterization of amphomycin effects on peptidoglycan and wall teichoic acid biosyntheses in Staphylococcus aureus. Sci Rep-uk 6, 31757 (2016).
8. Doerrler WT, Sikdar R, Kumar S & Boughner LA New Functions for the Ancient DedA Membrane Protein Family. J Bacteriol 195, 3–11 (2013). [PubMed: 23086209]
9. Typas A, Banzhaf M, Gross CA & Vollmer W From the regulation of peptidoglycan synthesis to bacterial growth and morphology. Nat Rev Microbiol 10, 123–136 (2012).

10. Piepenbreier H, Diehl A & Fritz G Minimal exposure of lipid II cycle intermediates triggers cell wall antibiotic resistance. Nat Commun 10, 2733 (2019). [PubMed: 31227716]
11. Barreteau H et al. Quantitative high-performance liquid chromatography analysis of the pool levels of undecaprenyl phosphate and its derivatives in bacterial membranes. J Chromatogr B 877, 213–220 (2009).
12. Dobihal GS, Flores-Kim J, Roney IJ, Wang X & Rudner DZ The WalR-WalK signaling pathway modulates the activities of both CwlO and LytE through control of the peptidoglycan deacetylase PdaC in Bacillus subtilis. J Bacteriol JB0053321 (2021) doi:10.1128/jb.00533-21.
13. Viklund H, Granseth E & Elofsson A Structural Classification and Prediction of Reentrant Regions in α-Helical Transmembrane Proteins: Application to Complete Genomes. J Mol Biol 361, 591–603 (2006). [PubMed: 16860824]
14. Eiamphungporn W & Helmann JD The Bacillus subtilis σM regulon and its contribution to cell envelope stress responses. Mol Microbiol 67, 830–848 (2008). [PubMed: 18179421]
15. Helmann JD Bacillus subtilis extracytoplasmic function (ECF) sigma factors and defense of the cell envelope. Curr Opin Microbiol 30, 122–132 (2016). [PubMed: 26901131]
16. Santiago M et al. Genome-wide mutant profiling predicts the mechanism of a Lipid II binding antibiotic. Nat Chem Biol 14, 601–608 (2018). [PubMed: 29662210]
17. Forrest LR Structural Symmetry in Membrane Proteins*. Biophysics 44, 311–337 (2015).
18. Brunner JD, Lim NK, Schenck S, Duerst A & Dutzler R X-ray structure of a calcium-activated TMEM16 lipid scramblase. Nature 516, 207–212 (2014). [PubMed: 25383531]
19. Morra G et al. Mechanisms of Lipid Scrambling by the G Protein-Coupled Receptor Opsin. Structure 26, 356–367.e3 (2018). [PubMed: 29290486]
20. Pomorski T & Menon AK Lipid flippases and their biological functions. Cell Mol Life Sci Cmls 63, 2908–2921 (2006). [PubMed: 17103115]
21. MURAMATSU Y, ISHII MM & INUKAI M Studies on Novel Bacterial Translocase I Inhibitors, A-500359s. J Antibiotics 56, 253–258 (2003).
22. Zallot R, Oberg N & Gerlt JA The EFI Web Resource for Genomic Enzymology Tools: Leveraging Protein, Genome, and Metagenome Databases to Discover Novel Enzymes and Metabolic Pathways. Biochemistry-us 58, 4169–4182 (2019).
23. Brindley DN & Waggoner DW Mammalian Lipid Phosphate Phosphohydrolases*. J Biol Chem 273, 24281–24284 (1998). [PubMed: 9733709]
24. Ghachi ME, Derbise A, Bouhss A & Mengin-Lecreulx D Identification of Multiple Genes Encoding Membrane Proteins with Undecaprenyl Pyrophosphate Phosphatase (UppP) Activity in Escherichia coli *. J Biol Chem 280, 18689–18695 (2005). [PubMed: 15778224]
25. Ghachi ME, Bouhss A, Blanot D & Mengin-Lecreulx D The bacA Gene of Escherichia coli Encodes an Undecaprenyl Pyrophosphate Phosphatase Activity*. J Biol Chem 279, 30106–30113 (2004). [PubMed: 15138271]
26. Jarrell KF et al. N-Linked Glycosylation in Archaea: a Structural, Functional, and Genetic Analysis. Microbiol Mol Biol R 78, 304–341 (2014).
27. Wu C-H et al. Bacillus subtilis YngB contributes to wall teichoic acid glucosylation and glycolipid formation during anaerobic growth. J Biological Chem 296, 100384 (2021).
28. Kuru E, Tekkam S, Hall E, Brun YV & Nieuwenhze MSV Synthesis of fluorescent D-amino acids and their use for probing peptidoglycan synthesis and bacterial growth in situ. Nat Protoc 10, 33–52 (2015). [PubMed: 25474031]
29. Panchuk-Voloshina N et al. Alexa Dyes, a Series of New Fluorescent Dyes that Yield Exceptionally Bright, Photostable Conjugates. J Histochem Cytochem 47, 1179–1188 (1999). [PubMed: 10449539]
30. Hapuarachchige S et al. Design and Synthesis of a New Class of Membrane-Permeable Triazaborolopyridinium Fluorescent Probes. J Am Chem Soc 133, 6780–6790 (2011). [PubMed: 21473622]
31. Grimm JB et al. A general method to improve fluorophores for live-cell and single-molecule microscopy. Nat Methods 12, 244–250 (2015). [PubMed: 25599551]

32. Sikdar R & Doerrler WT Inefficient Tat-Dependent Export of Periplasmic Amidases in an Escherichia coli Strain with Mutations in Two DedA Family Genes. J Bacteriol 192, 807–818 (2010). [PubMed: 19880597]
33. Kumar S & Doerrler WT Members of the Conserved DedA Family Are Likely Membrane Transporters and Are Required for Drug Resistance in Escherichia coli. Antimicrob Agents Ch 58, 923–930 (2014).
34. Boughner LA & Doerrler WT Multiple deletions reveal the essentiality of the DedA membrane protein family in Escherichia coli. Microbiology+ 158, 1162–1171 (2012). [PubMed: 22301910]
35. Panta PR & Doerrler WT A Burkholderia thailandensis DedA Family Membrane Protein Is Required for Proton Motive Force Dependent Lipid A Modification. Front Microbiol 11, 618389 (2021). [PubMed: 33510730]
36. Li YE et al. TMEM41B and VMP1 are scramblases and regulate the distribution of cholesterol and phosphatidylserine. J Cell Biology 220, e202103105 (2021).
37. Huang D et al. TMEM41B acts as an ER scramblase required for lipoprotein biogenesis and lipid homeostasis. Cell Metab 33, 1655–1670.e8 (2021). [PubMed: 34015269]
38. Ghachi ME et al. Crystal structure of undecaprenyl-pyrophosphate phosphatase and its role in peptidoglycan biosynthesis. Nat Commun 9, 1078 (2018). [PubMed: 29540682]
39. Eastman SJ, Hope MJ & Cullis PR Transbilayer transport of phosphatidic acid in response to transmembrane pH gradients. Biochemistry-us 30, 1740–1745 (1991).
40. Sit B et al. Candidate undecaprenyl phosphate translocases enable conditional microbial fitness and pathogenesis. Biorxiv 2022.02.04.479082 (2022) doi:10.1101/2022.02.04.479082.
41. Tzeng Y-L et al. Cationic Antimicrobial Peptide Resistance in Neisseria meningitidis. J Bacteriol 187, 5387–5396 (2005). [PubMed: 16030233]
42. Tiwari V et al. A Klebsiella pneumoniae DedA family membrane protein is required for colistin resistance and for virulence in wax moth larvae. Sci Rep-uk 11, 24365 (2021).
43. Moskowitz SM, Ernst RK & Miller SI PmrAB, a Two-Component Regulatory System of Pseudomonas aeruginosa That Modulates Resistance to Cationic Antimicrobial Peptides and Addition of Aminoarabinose to Lipid A. J Bacteriol 186, 575–579 (2004). [PubMed: 14702327]
44. Short FL et al. Genomic Profiling Reveals Distinct Routes To Complement Resistance in Klebsiella pneumoniae. Infect Immun 88, e00043–20 (2020). [PubMed: 32513855]
45. Paczosa MK et al. Transposon Mutagenesis Screen of Klebsiella pneumoniae Identifies Multiple Genes Important for Resisting Antimicrobial Activities of Neutrophils in Mice. Infect Immun 88, (2020).
46. Sanchez-Larrayoz AF et al. Complexity of Complement Resistance Factors Expressed by Acinetobacter baumannii Needed for Survival in Human Serum. J Immunol 199, 2803–2814 (2017). [PubMed: 28855313]

## Additional references

1. Youngman P, Perkins JB & Losick R Construction of a cloning site near one end of Tn917 into which foreign DNA may be inserted without affecting transposition in Bacillus subtilis or expression of the transposon-borne erm gene. Plasmid 12, 1–9 (1984). [PubMed: 6093169]
2. Dobihal GS, Flores-Kim J, Roney IJ, Wang X & Rudner DZ The WalR-WalK signaling pathway modulates the activities of both CwlO and LytE through control of the peptidoglycan deacetylase PdaC in Bacillus subtilis. J Bacteriol JB0053321 (2021) doi:10.1128/jb.00533-21.
3. Meeske AJ et al. MurJ and a novel lipid II flippase are required for cell wall biogenesis in Bacillus subtilis. Proc National Acad Sci 112, 6437–6442 (2015).
4. Santiago M et al. Genome-wide mutant profiling predicts the mechanism of a Lipid II binding antibiotic. Nat Chem Biol 14, 601–608 (2018). [PubMed: 29662210]
5. Zallot R, Oberg N & Gerlt JA The EFI Web Resource for Genomic Enzymology Tools: Leveraging Protein, Genome, and Metagenome Databases to Discover Novel Enzymes and Metabolic Pathways. Biochemistry-us 58, 4169–4182 (2019).

6. Singh M, Chang J, Coffman L & Kim SJ Solid-state NMR characterization of amphomycin effects on peptidoglycan and wall teichoic acid biosyntheses in Staphylococcus aureus. Sci Rep-uk 6, 31757 (2016).

7. Wang X et al. Condensin promotes the juxtaposition of DNA flanking its loading site in Bacillus subtilis. Gene Dev 29, 1661–1675 (2015). [PubMed: 26253537]

8. Fujita M & Sadaie Y Rapid isolation of RNA polymerase from sporulating cells of Bacillus subtilis. Gene 221, 185–190 (1998). [PubMed: 9795209]

9. Mendler K et al. AnnoTree: visualization and exploration of a functionally annotated microbial tree of life. Nucleic Acids Res 47, 4442–4448 (2019). [PubMed: 31081040]

10. Sievers F et al. Fast, scalable generation of high-quality protein multiple sequence alignments using Clustal Omega. Mol Syst Biol 7, 539–539 (2011). [PubMed: 21988835]

11. Robert X & Gouet P Deciphering key features in protein structures with the new ENDscript server. Nucleic Acids Res 42, W320–W324 (2014). [PubMed: 24753421]

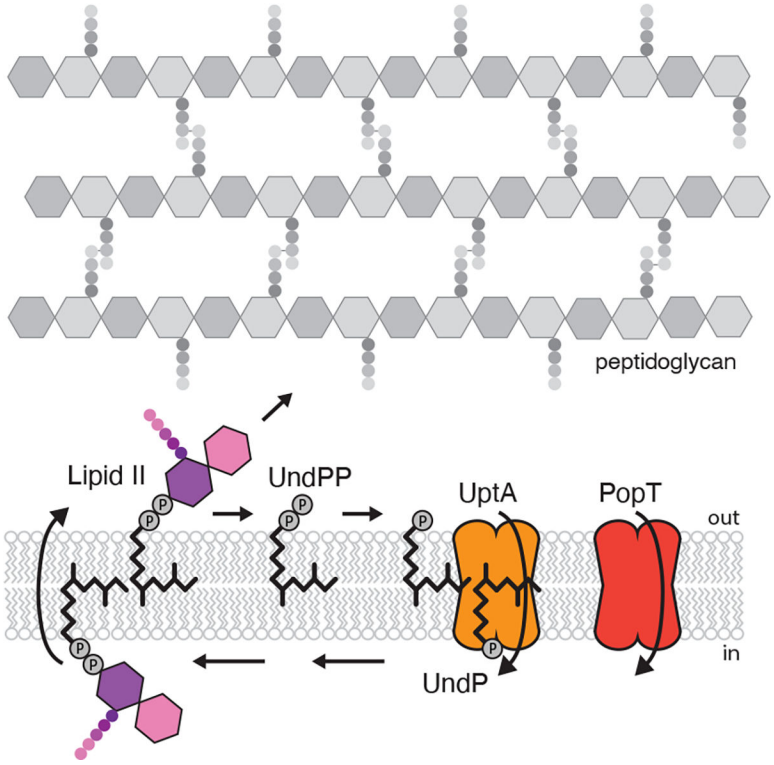


**Figure 1. UptA and PopT complete the lipid II cycle.**

Schematic of the lipid II cycle in peptidoglycan synthesis highlighting the role of UptA and PopT in recycling undecaprenyl-phosphate (UndP).

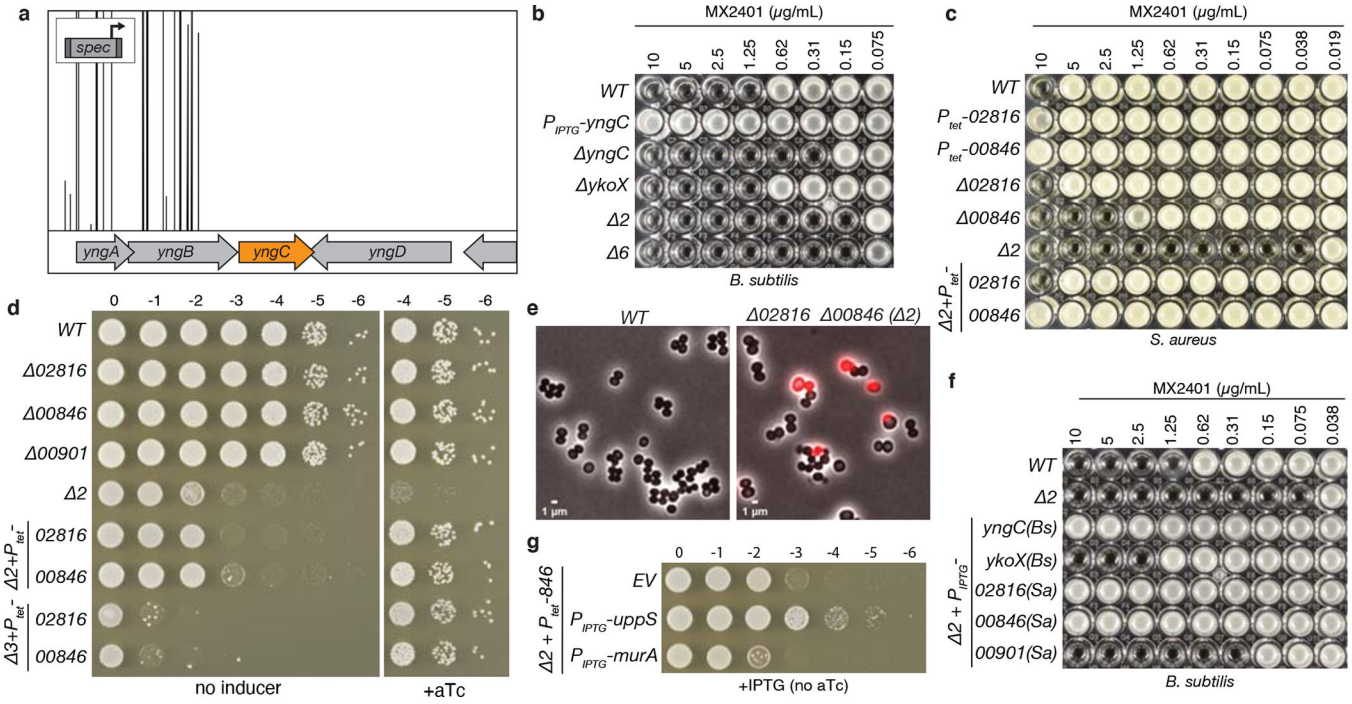


**Figure 2. DedA and DUF368 family members provide resistance to UndP-targeting antibiotics.**

**(a)** A transposon-sequencing screen for MX2401-resistance mutants identifies *yngC*. Transposon insertion profile at the indicated *B. subtilis* genomic region is shown. Each vertical line indicates a Tn insertion site; its height reflects the number of sequencing reads at this position. All transposons in this region were inserted with the outward facing promoter facing *yngC* as indicated in the schematic. Most insertion sites had >20,000 reads but the window size was scaled to 5,000 to highlight the absence of reads in the neighboring genes. **(b)** Minimum inhibitory concentration (MIC) assay of the indicated *B. subtilis* strains. **(c)** MIC assay of the indicated *S. aureus* strains. **(d)** Spot-dilution assays of the indicated *S. aureus* strains on TSA with or without 100 ng/mL anhydrotetracycline (+aTc). **(e)** Representative images of wild-type and *Δ00846 Δ02816* (*Δ2*) *S. aureus* cells. Overlays of phase-contrast and propidium iodide fluorescence are shown. **(f)** MIC assays of the indicated *B. subtilis* strains over-expressing DedA and DUF368 family members from *B. subtilis* and *S. aureus*. **(g)** Spot-dilutions of the indicated *S. aureus* strains harboring an empty vector (EV) or a vector with an IPTG-regulated promoter fused to *uppS* or *murA*.

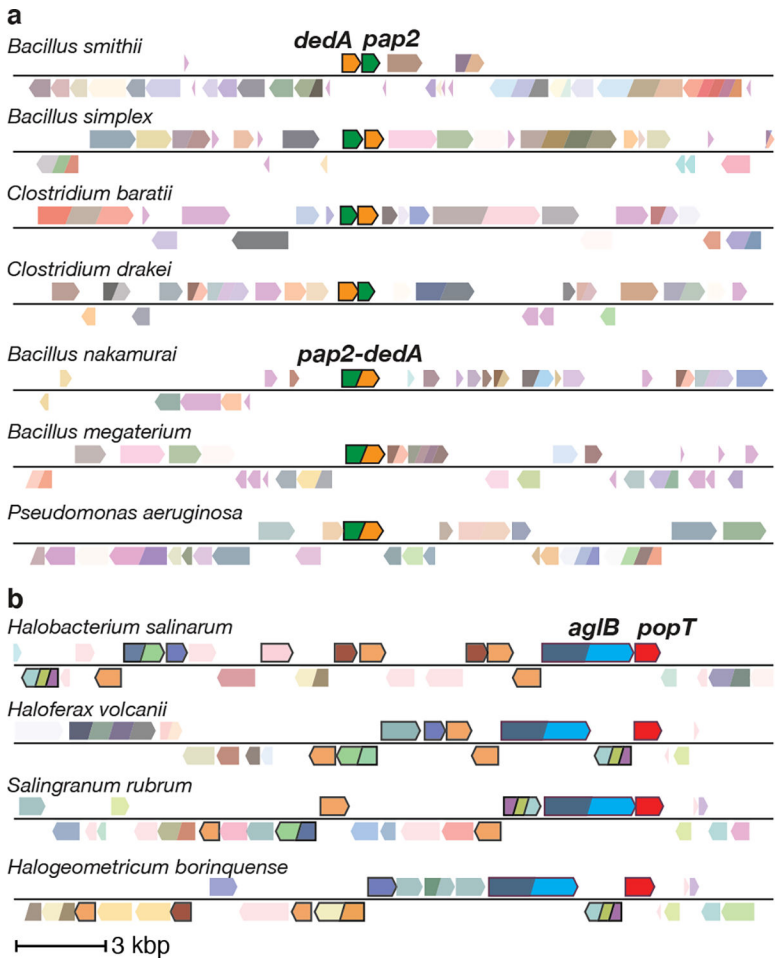


**Figure 3. Gene neighborhood analyses for DedA and DUF368 family members.**

Representative genomic neighborhood diagrams highlight the synteny or fusion of a *dedA* gene with a gene encoding a PAP2 lipid phosphatase **(a)** and the synteny of *duf368* with genes involved in archaeal N-linked protein glycosylation pathways **(b)**. ~1.3% of all *dedA* genes are fused to *pap2* genes. The gene encoding the oligosaccharyltransferase AglB is shown in blue and other genes in the glycosylation pathway are highlighted by black borders. 37% of *duf368* genes are present in gene clusters encoding protein glycosylation pathways.

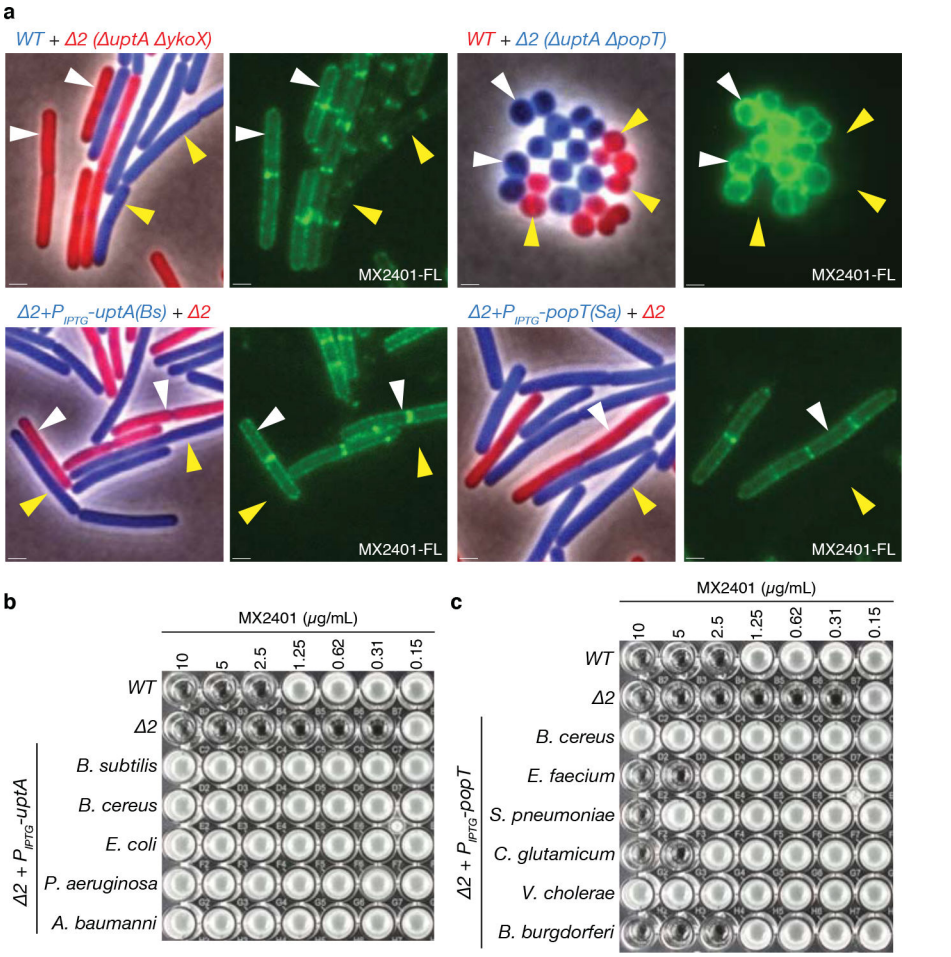


**Figure 4. UptA and PopT are broadly conserved UndP transporters.**

**(a)** Representative microscopy images of the indicated *B. subtilis* or *S. aureus* strains. Two strains expressing different fluorescent proteins (*B. subtilis*) or labeled with different fluorescent D-amino acids (*S. aureus*) were mixed and then stained with fluorescent MX2401 (MX2401-FL). The left panels show overlays of phase-contrast and fluorescent images in the red and blue channels to distinguish the two strains. The right panels show MX2401-FL staining. Yellow carets highlight wild-type cells or cells over-expressing UptA(*Bs*) or PopT(*Sa*). White carets highlight cells lacking the UndP transporters. Scale bar, 1μm. MIC assays of *B. subtilis* strains over-expressing UptA **(b)** or PopT **(c)** homologs from the indicated bacteria.